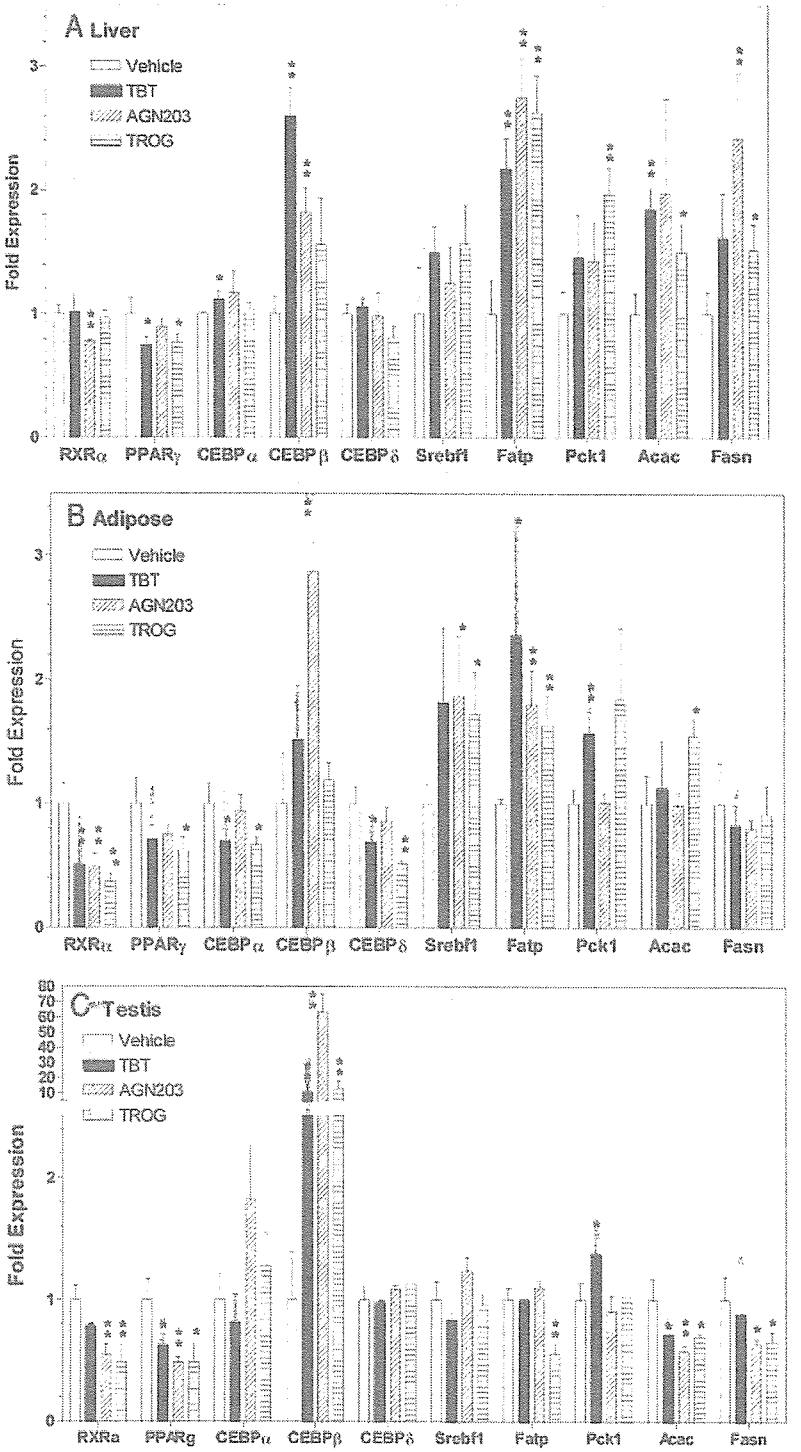

Fig. 3. *In Vivo* Induction of Adipogenic Modulators and RXR:PPARγ Target Genes

C57BL/6 male mice (three animals per treatment) were dosed with TBT (0.3 mg/kg b.w.), AGN195203 (0.3 mg/kg), troglitazone (3 mg/kg b.w.), or vehicle (corn oil) only by ip injection. Animals were killed after 24 h and dissected and cDNA was prepared from liver, epididymal fat pad, or testis for quantitative real-time PCR analysis. Expression levels were normalized to histone Hist2h4 and shown as the average fold change ± SEM (n = 3) compared with vehicle (corn oil) controls. Control *vs.* ligand treatments were analyzed by the unpaired Student's *t* test: *, $P < 0.1$; **, $P < 0.05$. TROG, Troglitazone.

with Oil Red O to assess changes in total tissue lipid accumulation. TBT exposure caused a disorganization of hepatic (Fig. 4, A and B) and gonadal (Fig. 4, C and D) architecture and significantly increased Oil Red O staining in treated animals *vs.* controls. Liver sections exhibited signs of steatosis consistent with the mis-

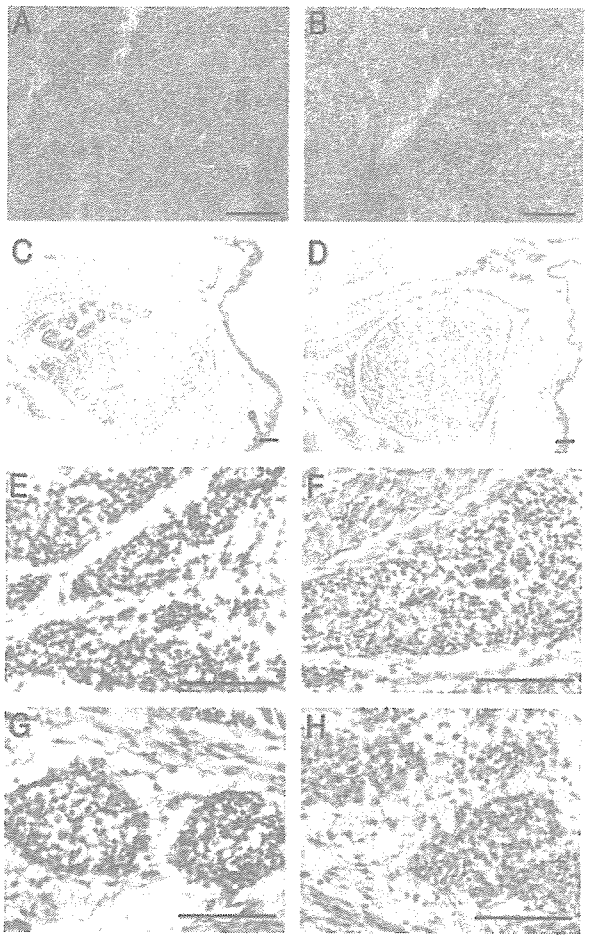

Fig. 4. *In Utero* Exposure to TBT Increases Adiposity in Mouse Liver, Testis, and Adipose Depots

Histological sections (12 μm) of newborn mouse liver (A and B), testis (C and D), inguinal adipose (E and F) and mammary adipose (G and H) stained with Oil Red O and counterstained with hematoxylin following *in utero* exposure to vehicle only (sesame oil) (A, C, E, and G) or 0.5 mg/kg b.w. TBT (B, D, F, and H) given s.c. daily from E12–18. *Scale bar*, 100 μm.

regulation of fatty acid uptake and synthesis observed using molecular markers. In addition, Oil Red O positive staining in mammary and inguinal adipose (Fig. 4, E–H) tissues was dramatically elevated, reflecting either an increase in lipid accumulation or an increase in mature adipocytes.

To determine whether exposure induced long-term changes in growth or adipose tissue, we followed mice from birth to adulthood after *in utero* exposure to TBT as indicated above. At birth, mice were cross-fostered to unexposed dams, and total body weight was recorded until 10 wk of age (Fig. 5A). Growth curves for male and female pups showed a slight trend for lower total body weight consistent with published observations (9) but were not statistically significant at 10 wk [control *vs.* TBT: male, 26.00 g ± 0.70 (n = 9) *vs.* 25.53 g ± 0.39 (n = 10), $P = 0.583$; female, 21.22 g ± 0.41 (n = 10), *vs.* 20.24 g ± 0.24 (n = 10), $P = 0.0529$]. Males were killed at 10 wk and epididymal fat pads were weighed (Fig. 5B). Adipose mass in TBT-treated males was increased significantly by 20% over controls [control *vs.* TBT: 0.30 g ± 0.020 (n = 9) *vs.* 0.36 g ± 0.018 (n = 10), $P = 0.0374$]. These data support the conclusion that TBT can increase body adiposity without overtly increasing total body weight. Similar lipid accumulation and changes in adipose tissue mass have also been observed after TZD or rexinoid treatment (55–57).

We had previously observed that TBT activated *Xenopus* RXRs (Table 1) and reasoned that the strong conservation in vertebrate nuclear receptor signaling pathways should result in consistent responses to organotin and RXR/PPARγ ligands across diverse vertebrate species. We therefore tested chronic exposure to environmentally relevant low doses of TBT (1–10 nM), the RXR-specific ligands LG100268 and AGN195203 (10–100 nM), troglitazone (0.1–1 μM), and estradiol (1–10 nM) on developing *X. laevis* tadpoles from stage 48 to metamorphs. To determine the effectiveness of these doses in *X. laevis* tadpoles, we used aromatase expression as a molecular marker because activity and expression are sensitive to endocrine disruption by organotins and RXR/PPARγ ligands in mammals (17, 18). *Xenopus* aromatase expression was similarly repressed 2- to 3-fold by 10 nM TBT, AGN195203, LG100268, or 1 μM troglitazone at stage 56 tadpoles (Fig. 6A) and at all subsequent stages. Despite significant ligand-induced aromatase down-regulation, neither sex ratios nor the time required to reach metamorphosis was altered (data not shown). *Xenopus* liver and kidney also exhibited no gross structural abnormalities at the doses given.

However, consistent with the testis and adipose results from mice presented above, we observed a dose-dependent increase in ectopic adipocyte formation posterior to the fat bodies in and around the gonads of both sexes after TBT or RXR/PPARγ ligand exposure (Fig. 6B). In contrast, estradiol-treated animals did not show increased adipocyte formation compared with controls. At 10 nM TBT, 10 nM AGN195203, or 1 μM troglitazone, ectopic adipocytes were observed in approximately 45–60% of animals. At the highest dose of TBT in males, testicular tissue was interspersed with, or replaced by, adipocytes along the anterior-posterior axis (Fig. 6, D, E, and G).

The concordant changes observed in *Xenopus* aromatase expression, gonadal adipocyte formation, and increased murine adiposity after exposure to TBT, RXR and PPARγ ligands are therefore consistent with a common mechanism of action through RXR:PPARγ activation, supporting the conclusion that endocrine disruption via nuclear receptor transcriptional regulation is a novel and key feature of organotin toxicity.

DISCUSSION

We have shown above that TBT is a potent inducer of adipogenesis, *in vitro* and *in vivo*, by acting as a novel,

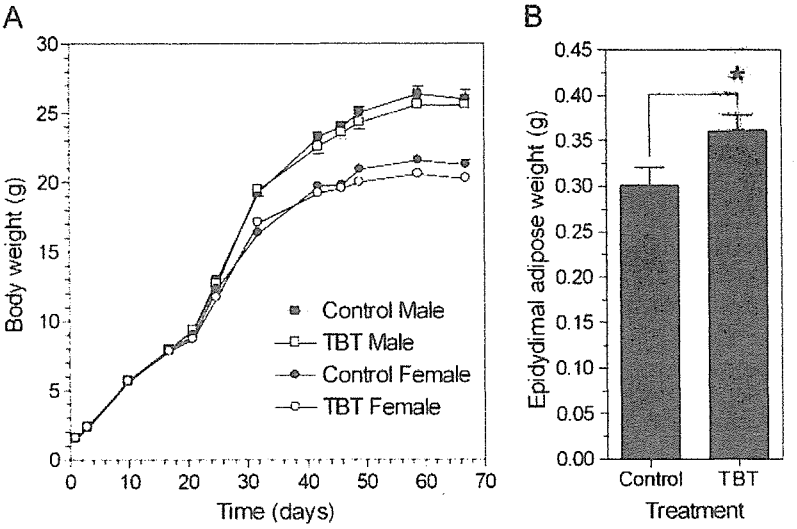

Fig. 5. *In Utero* Exposure to TBT Increases Adipose Mass But Not Body Weight in Adult Mice

A, Growth curves of C57BL/6 male and female pups exposed to control (sesame oil) or TBT *in utero* (E12–18). Data are mean ± SEM (n = 10). B, Epididymal fat pad weights from control or TBT-treated males at 10 wk. *, Epididymal adipose mass from exposed males was approximately 20% greater [control *vs.* TBT: 0.30 g ± 0.020 (n = 9) *vs.* 0.36 g ± 0.018 (n = 10); *, $P = 0.0374$). Data represent mean ± SEM (n = 9–10).

high-affinity xenobiotic ligand for RXRα and PPARγ. The ability of organotins to bind and activate these receptors, in particular the RXRs, which exhibit very restricted ligand specificity, is unexpected given the radically different chemical composition and three-dimensional molecular structure of organotins when compared with known natural and synthetic nuclear receptor ligands. Typically, RXR ligands comprise a carboxylic acid functional group and a three-dimensional molecular shape that mimics 9-*cis* RA. Structure-activity profiles indicate distinct structural preferences for organotins but also a relatively broad accommodation for agonist activity that is not easily reconciled with the classical ligand-binding model. Organotins may therefore interact somewhat differently than previously described RXR/PPARγ ligands with receptor LBDs to induce productive conformational changes required for coactivator recruitment. However, the binding data indicate that TBT is a potent and efficacious ligand for both RXRs and PPARγ that interacts, at least partially, with the same receptor-binding sites of other high-affinity ligands and promotes the necessary cofactor interactions required for agonist activation. In the study of Kanayama *et al.* (24), TBT was only effective in coactivator recruitment assays with PPARγ above 10 μM *in vitro*. However, in accord with our findings, they show that TBT activated PPARγ significantly at nanomolar concentrations in transfection assays. This may reflect a limitation of preference in the cofactor used *in vitro*. Alternatively, the lower maximal activation observed with TBT on PPARγ in cells (~30% at 100 nM TBT cf troglitazone) is consistent with one of two possibilities: either nonspecific cellular toxicity at high levels or activation as a partial agonist.

The ability of TBT to act as a dual ligand for permissive heterodimers such as RXRα:PPARγ, which can be activated by specific ligands for either receptor, also raises the possibility for additive or synergistic effects that might increase the potency of these compounds *in vivo* at low doses for this specific signaling pathway. Of note is that receptor activation is observed at nanomolar concentrations, whereas other mechanisms of toxicity and endocrine disruption, *e.g.* direct inhibition of aromatase activity, typically occur in the micromolar range. Furthermore, the activation of other permissive RXR heterodimeric partners, *e.g.* LXR and NURR1, suggests that organotins may act more widely to disrupt multiple nuclear receptor-mediated hormonal signaling pathways.

The biological consequences of organotin activation of the RXR:PPARγ signaling pathway are predictable and should follow known aspects of RXR/PPARγ biology. The RXR:PPARγ pathway plays a key role in adipocyte differentiation and energy storage, and is central to the control of whole-body metabolism (58). PPARγ activation increases the expression of genes that promote fatty acid storage and represses genes that induce lipolysis in adipocytes in white adipose tissue (59). PPARγ such as the thiazolidinediones can modulate insulin sensitivity due to these effects on the adipocyte, reversing insulin resistance in the whole body by sensitizing the muscle and liver tissue to insulin (60). However, a consequence of this increase in whole-body insulin sensitivity is that fat mass is increased through the promotion of triglyceride storage in adipocytes. Evidence is also mounting that depot-specific remodeling and adipocyte numbers increase after thiazolidinedione treatment (55–57). Therefore, PPARγ agonists comprise a class of phar-

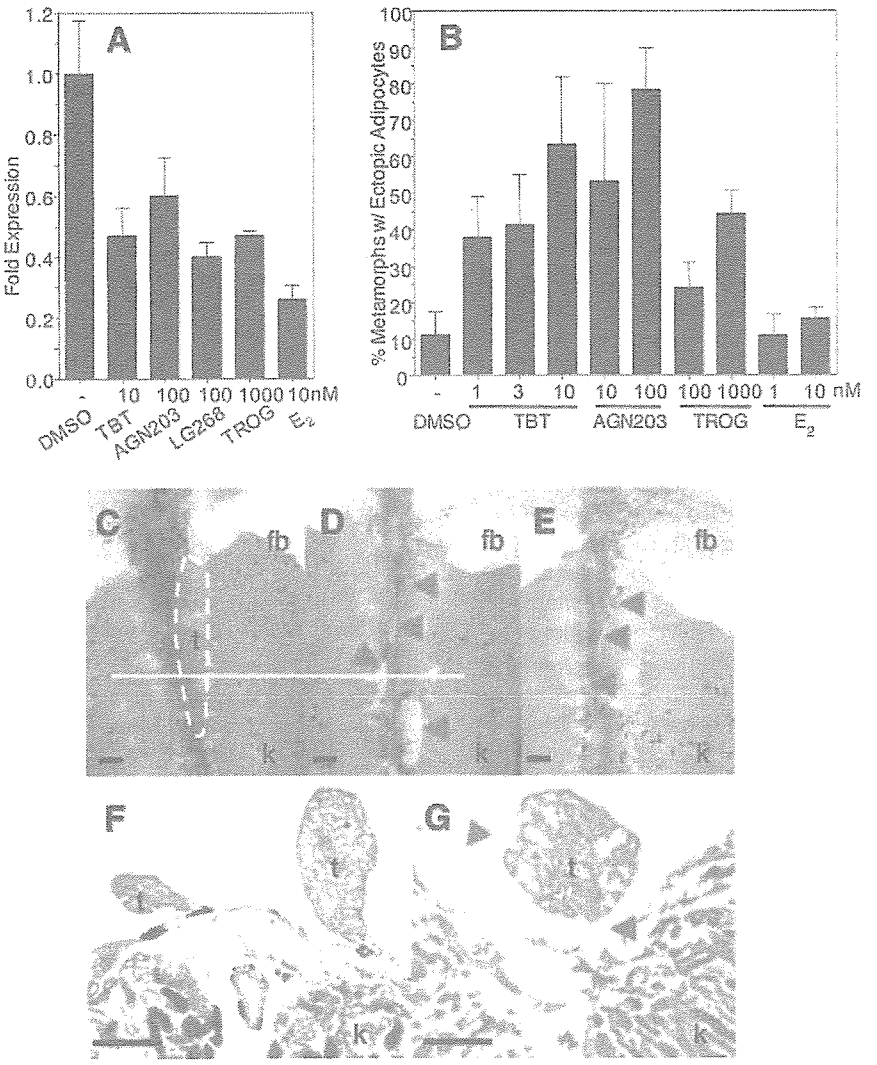

Fig. 6. Endocrine Disruption of RXR:PPARγ Signaling and Ectopic Induction of Adipocytes in *X. laevis* by TBT

A, Expression levels of *Xenopus* aromatase (XCYP19) were determined in tadpoles (stage 56) by quantitative real-time PCR after 24-h exposure to vehicle only (DMSO) or the indicated ligands. Expression was normalized to *Xenopus* EF1α and expressed as average fold change in expression ± SEM (n = 9) relative to vehicle controls. B, *X. laevis* tadpoles were dosed weekly under static renewal conditions with indicated ligands from stage 48 (before gonadogenesis) until stage 64 (metamorphic climax). Metamorphs (stage 66) were scored for ectopic adipocyte patches on gonads and urogenital ducts. Data are shown as the percentage of metamorphs exhibiting ectopic adipocyte patches posterior to the fat bodies; mean ± SD from triplicate tanks. C–E, Dissecting microscope photographs of kidneys (k), testis (t), and fat bodies (fb) from DMSO control, 10 nM TBT, and 1 μM troglitazone-treated male metamorphs. Multiple ectopic adipocyte patches (*red arrows*) are present posterior to the fat bodies along the anterior-posterior axis of gonads in TBT (D)- and troglitazone (E)-treated animals but not controls (C). Histological sections of kidneys and gonads from the same control (F) and 10 nM TBT (G)-treated males at the level indicated by the *white line* in C and D. Gonadal and connective tissue was either completely replaced by, or interspersed with, adipocytes (*red arrows*) in TBT-treated animals. Sections were developed with Mallory's trichrome stain. *Scale bars*, 100 μm.

maceutical therapies for type 2 diabetes that can also promote obesity by increasing fat storage. Likewise, RXR ligands also act as insulin-sensitizing agonists in rodents (61), underscoring the permissive nature of the PPARγ:RXR heterodimer and the potential effects on diabetes and obesity of both PPARγ and RXR agonists.

Our data are consistent with recent studies that organotins can mediate some of their endocrine disruption effects by transcriptional regulation through nuclear receptors, in particular RXR:PPARγ signaling (17–19, 24). Consequently, TBT exposure can promote adipocyte differentiation in the same manner as other RXR or PPARγ ligands *in vitro* using the standard murine 3T3-L1 cell model and *in vivo* through increased adiposity after intrauterine organotin exposure in newborn mice. It is currently unknown whether the increased adiposity *in vivo* results from an increase

in adipocyte precursor cell number, enhanced adipocyte differentiation from the same number of precursors, an increase in adipocyte size without an increase in number, or some combination of these.

The prevailing epidemiological data ascribe high-density caloric and/or fatty diets coupled with decreased physical activity as the root causes for the rise in obesity rates in the general population (62). The contribution of genetic components is less clear. Although genetic variation contributes to an individual's propensity to develop obesity, the rapid worldwide increase in obesity suggests that interaction with the modern environment exposes inherent genetic differences. The Barker hypothesis postulates that *in utero* fetal nutritional status is a potential risk factor for metabolic syndrome diseases (63–67). In this view, developmental metabolic programming of a thrifty phenotype limits the range in adaptive responses to the environment, *e.g.* diet and exercise, in later life (68). Experimental evidence from animal models lends support to this hypothesis (69). Plausible mechanisms include imprinting of obesity-sensitive hormonal pathways or changes in cell type and number, *e.g.* adipocytes, established during development.

Others, however, argue that the environment plays another role in obesity. Because the increase in obesity rates parallels the rapid growth in the use of industrial chemicals over the past 40 yr, it is plausible and provocative to associate *in utero* or chronic lifetime exposure to chemical triggers present in the modern environment with this epidemic. Hence, an "obesogen" model predicts the existence of xenobiotic chemicals that inappropriately regulate lipid metabolism and adipogenesis to promote obesity. Several recent studies serve as proof-of-principle for such a hypothesis. Environmental estrogens such as bisphenol A and nonylphenol, for instance, can promote adipocyte differentiation or proliferation in murine cell lines (70, 71). Furthermore, epidemiological studies link maternal smoking during pregnancy to an elevated risk of childhood obesity (72–76).

Seen in this context, we propose that organotins such as TBT and its congeners are chemical stressors or obesogens that activate RXR:PPARγ signaling to promote long-term changes in adipocyte number and/or lipid homeostasis after developmental or chronic lifetime exposure.

MATERIALS AND METHODS

Plasmids and Transfections

pCMX-GAL4 and pCMX-VP16 plasmid fusion constructs to nuclear receptor LBDs and coactivators [GAL4-hRARα, hRXRα, -xRXRα/γ, -hPPARγ, -mPPARα, -human steroid and xenobiotic receptor (SXR), -NURR1, -VDR, -LXR, -hACTR, -hPPAR-binding protein (PBP), -human steroid receptor coactivator-1 (SRC-1), human transcriptional intermediary factor 2 (TIF2)] have been previously described (77–82). Transfections were performed in Cos7 cells (transformed green monkey kidney fibroblast cell line) essentially as described elsewhere (83) using MH200-x4-TK-Luc as reporter and normalized to pCMX-β-galactosidase controls. Briefly, Cos7 cells were seeded at 5000 cells per well in 96-well tissue culture plates in 10% fetal bovine serum/DMEM and transfected for 8 h with 11 μg/plate of DNA/calcium phosphate precipitate mix (MH200x4-TK-Luc-CMX-β-galactosidase-nuclear receptor/coactivator effector(s) at a ratio of 5:5:1). Cells were washed free of precipitate with PBS and media were replaced with serum-free insulin, transferrin, lipid, bovine serum albumin supplemented (ITLB)/DMEM (84) plus ligands for an additional 24 h before assays for luciferase and β-galactosidase activity. All transfection data points were performed in triplicate, and all experiments were repeated at least three times.

Quantitative Real-Time PCR Analyses

Total cellular RNA from C57BL/6 mouse and *X. laevis* tissues was isolated with Trizol reagent and reversed transcribed with oligo dT and Superscript II (Invitrogen, San Diego, CA) according to the manufacturer's instructions. Triplicate cDNA samples (50 ng/reaction) were analyzed by quantitative real-time PCR on a DNA Engine Opticon thermal cycler [MJ Research (Watertown, MA)/Bio-Rad Laboratories (Hercules, CA)] using SYBR Green chemistry (PerkinElmer Life Sciences, Wellesley, MA). Fold changes in expression levels were calculated after normalization to histone Hist2h4 using the Δ-Δ cycle threshold method (85). Gene-specific primers were as follows. Hist2h4 forward (F): 5′-CCCGTGGTGTGCTGAAGGTGTT-3′; reverse (R), 5′-GAATTGAAGCGGCGGCGTCTA-3′; RXRα F: 5′-CGGCTGCTCAGGGTACTTGTGTTT-3′; R, 5′-CGGCTGCTCAGGGTACTTGTGTTT-3′; PPARγ F: 5′-TGGGTGAAACTCTGGGAGATTC-3′; R, 5′-AATTTCTTGTGAAGTGCTCATAGGC-3′; C/EBPα F: 5′-CCAAGAAGTCGGTGGACAAGA-3′; R, 5′-CGGTCATTGTCACTGGTCAACT-3′; C/EBPβ F: 5′-GCCCGCCGCCTTTAGACC-3′; R, 5′-CGCTCGTGCTCGCCAATG-3′; C/EBPδ F: 5′-AACCCGCGGCCTTCTACGAG-3′; R, 5′-ACGGCGGCCATGGAGTCAAT-3′; aP2 F: 5′-GAATTCGATGAAATCACCGCA-3′; R, 5′-CTCTTTATTGTGGTCGACTTTCCA-3′; FATP F: 5′-AGCCGCTTCTGGGATGACTGTGT-3′; R, 5′-ACCGAAGCGCTGCGTGAACTC-3′; ACS F: 5′-CCCAGCCAGTCCCCACCAG-3′; R, 5′-CACACCACTCAGGCTCACACTCGT-3′; FASN F: 5′-TCGGGTGTGGTGGGTTTGGTGAAT-3′; R, 5′-ACTTGGGGGCGTGAGATGTGTTGC-3′;ACAC F: 5′-G GATGGCAGCTCTGGAGGTGTATG-3′; R, 5′-TGTCCTTAAGCTGGCGGTGTTGTA; Pck1 F: 5′-CTGGCAGCATGGGGTGTTTGTAGG-3′; R, 5′-TGCCGAAGTTGTAGCCGAAGAAGG-3′; Srebf1 F: 5′-GCCCCTGCCCACCTCAAACCT-3′; R, 5′-ACTGGCACGGGCATCCTTCCTC-3′; *Xenopus* EF1α F: 5′-GATCCCAGGAAAGCCAATGTGC 3′; R, 5′-CCGGATCCTGCTGCCTTCTTCT-3′; *Xenopus* CYP19 (aromatase) F: 5′-GTCTGGATTAATGGCGAGGAAACA-3′; R, 5′-CTGATGAAGTATGGCCGAATGACC-3′.

Ligand Binding

Histidine-tagged RXRα LBD (H_6-RXRα LBDs) was expressed and purified from pET15b(+) vector in BL21(DE3) pLysS bacteria cultures after induction with 1 mM isopropyl-β-D-thiogalactopyranoside for 3 h at 37 C (86). Purified H_6-PPARγ was purchased from Invitrogen. Proteins were bound to 96-well Nickel Chelate Flashplates (PerkinElmer Life Sciences) at 100 μg/ml overnight at 4 C and washed five times with 200 μl/well Flashplate Assay Buffer (20 mM HEPES, pH 7.9; 100 mM KCl, 0.1% cholamidopropyldimethylammonio-2-hydroxy-1-propanesulfonate, 0.1 mM dithiothreitol). Competition assays typically used 1–5 nM [^{3}H]-9-*cis*-RA (PerkinElmer Life Sciences) or 10–50 nM [^{3}H]rosiglitazone (American Radiochemicals, Inc., St. Louis, MO) plus cold competitor ligands in Flashplate Assay Buffer at concentrations indicated in the figures. Plates were incubated at room temperature, pro-

tected from light, and read after 4 h on a Packard Topcount scintillation counter (Packard Instruments, Meriden, CT). Specific bound counts/min were determined by subtraction of counts/min from uncoated wells at each ligand concentration. Data were analyzed with GraphPad Prism 4.0 (GraphPad Software, Inc., San Diego, CA) using a one-site competition binding equation to determine K_i values for competitor ligands; K_d values of 1.4 and 41 nM for 9-*cis*-RA and rosiglitazone for their respective receptors were used in the calculations (87, 88).

3T3-L1 Cell Assays

3T3-L1 (American Type Culture Collection, Manassas, VA) cells were maintained as subconfluent cultures by passage every 3 d from cultures seeded at 5000 cells/cm^2 in 8% calf serum/DMEM. For differentiation assays, cells were seeded at 15×10^3 cells per well into 24-well tissue culture plates in 8% fetal bovine serum/DMEM, after which cultures were grown for 2 d and then treated with the indicated RXR, RAR, and PPAR ligands either with or without MDIT (100 μM 3-isobutyl-1-methylxanthine, 100 nM dexamethasone, 0.1 ng/ml insulin, and 2 nM T_3 thyroid hormone) induction cocktail. Media and ligand treatments were renewed every 2 d. After 1 wk, cells were scored for adipocyte differentiation by Oil Red O staining for lipid droplet accumulation. Cultures were washed with PBS, fixed with 10% formaldehyde for 15 min, washed with distilled water, and stained with filtered Oil Red O solution (4 g/liter, 60% isopropanol) for 15 min. Excess stain was removed by washing three times with distilled water. Three random fields from each well were photographed under phase contrast and analyzed in ImageJ. Images were converted into high-contrast black and white images to visualize lipid droplets and scored as the percentage area per field. Data are shown as the mean ± SEM from three wells per treatment. The method was validated by extraction of Oil Red O from stained cells into 100% isopropanol and quantitated by absorbance at 540 nm on a spectrophotometer.

In Vivo Animal Exposure Experiments

C57BL/6J mice were housed under a 12-h light, 12-h dark cycle. Pregnant mice were dosed by ip injection with TBT [0.05 or 0.5 mg/kg body weight (b.w.)] or vehicle (sesame oil) from embryonic d 12 (E12) every 24 h until the day before delivery. Neonates were killed at the day of delivery and analyzed. The samples were embedded in optimal cutting temperature embedding compound and sectioned (12 mm) using a cryostat. Sections were fixed on slides with 4% paraformaldehyde for 10 min and rinsed in PBS. The slides were then sequentially washed with distilled water and 60% of isopropanol and stained with Oil Red O (4 g/liter, 60% isopropanol). After washing with 60% isopropanol and distilled water, the slides were counterstained with hematoxylin. Sections were evaluated and photographed using a Zeiss microscope (Carl Zeiss, Thornwood, NY).

For long-term growth studies, pups were cross-fostered to unexposed C57BL/6 dams after birth, and litter sizes were kept constant at eight pups per dam (control, two male + two female; TBT treated, two male + two female). Animals were weaned at 3 wk of age and maintained on standard rodent chow. Total body weight was followed until 10 wk of age. Males were then killed, and epididymal fat pads were dissected and weighed.

X. laevis tadpoles were sorted at stage 48 (89) and maintained in 1-liter glass tanks in 20% Holtfreter's buffered salt solution (90) at a density of 10 tadpoles per tank on a diet of ground Tetramin Fish Flakes and spirulina. Compounds prepared in dimethylsulfoxide (DMSO) as 10^5-fold stock solutions were tested on triplicate tanks and dosed by static renewal after weekly water changes. Metamorphs at stage 64 were transferred to individual containers and fed frozen brine shrimp for 2 wk until stage 66. Froglets were euthanized with 250 mg/liter MS222 in 20% Holtfreter's solution and then scored for gonadal abnormalities and interrenal/gonadal adipocyte formation under a dissecting microscope. Kidneys with attached gonads and livers were fixed in 10% formalin-PBS, embedded in paraffin, and sectioned at 15 μm thickness. Sections were developed with Mallory's trichrome stain.

All animal experiments were approved and performed in accordance with Institutional Animal Care and Use Committee protocols.

Acknowledgments

We thank Drs. I. Blitz, K. Cho, C. Zhou, and T. Osborne for critical reading and comments on the manuscript, Dr. C. Li (Expression Technologies) for the H_6-RXRα LBD construct, and Dr. R. Chandraratna (Allergan Pharmaceuticals, Irvine, CA) for AGN203 and LG268).

Received September 8, 2005. Accepted March 30, 2006.

Address all correspondence and requests for reprints to: Bruce Blumberg, Department of Developmental and Cell Biology, University of California Irvine, 2113 McGaugh Hall, Irvine, California 92697-2300. E-mail: blumberg@uci.edu.

This work was supported by grants from the U.S. Environmental Protection Agency (STAR R830686) and National Institutes of Health (GM-60572) (to B.B.); from the Ministries of Education, Culture, Sports, Science and Technology, Environment and Health Labor and Welfare, Japan (to T.I.); and from the University of California Toxic Substance Research and Training Program (UC-37579) (to F.G.).

F.G., H.W., Z.Z., L.M., K.A., R.C., D.M.G., J.K., T.I. have nothing to declare. B.B. is a named inventor on U.S. patents US 5,861,274, US 6,200,802, and US 6,815,168.

REFERENCES

1. Appel KE 2004 Organotin compounds: toxicokinetic aspects. Drug Metab Rev 36:763–786
2. Golub M, Doherty J 2004 Triphenyltin as a potential human endocrine disruptor. J Toxicol Environ Health B Crit Rev 7:281–295
3. Blaber SJM 1970 The occurrence of a penis-like outgrowth behind the right tentacle in spent females of *Nucella lapillus*. Proc Malacolog Soc London 39:231–233
4. Gibbs P, Bryan G 1986 Reproductive failure in populations of the dog-whelk, *Nucella lapillus*, caused by imposex induced by tributyltin from antifouling paints. J Mar Biol Assoc UK 66:767–777
5. Matthiessen P, Gibbs P 1998 Critical appraisal of the evidence for tributyltin-mediated endocrine disruption in mollusks. Environ Toxicol Chem 17:37–43
6. Shimasaki Y, Kitano T, Oshima Y, Inoue S, Imada N, Honjo T 2003 Tributyltin causes masculinization in fish. Environ Toxicol Chem 22:141–144
7. McAllister BG, Kime DE 2003 Early life exposure to environmental levels of the aromatase inhibitor tributyltin causes masculinisation and irreversible sperm damage in zebrafish (*Danio rerio*). Aquat Toxicol 65:309–316
8. Omura M, Ogata R, Kubo K, Shimasaki Y, Aou S, Oshima Y, Tanaka A, Hirata M, Makita Y, Inoue N 2001 Two-generation reproductive toxicity study of tributyltin chloride in male rats. Toxicol Sci 64:224–232
9. Ogata R, Omura M, Shimasaki Y, Kubo K, Oshima Y, Aou S, Inoue N 2001 Two-generation reproductive toxicity

study of tributyltin chloride in female rats. J Toxicol Environ Health A 63:127–144
10. Boyer IJ 1989 Toxicity of dibutyltin, tributyltin and other organotin compounds to humans and to experimental animals. Toxicology 55:253–298
11. Heidrich DD, Steckelbroeck S, Klingmuller D 2001 Inhibition of human cytochrome P450 aromatase activity by butyltins. Steroids 66:763–769
12. Cooke GM 2002 Effect of organotins on human aromatase activity in vitro. Toxicol Lett 126:121–130
13. Powers MF, Beavis AD 1991 Triorganotins inhibit the mitochondrial inner membrane anion channel. J Biol Chem 266:17250–17256
14. Gennari A, Viviani B, Galli CL, Marinovich M, Pieters R, Corsini E 2000 Organotins induce apoptosis by disturbance of [Ca(2+)](i) and mitochondrial activity, causing oxidative stress and activation of caspases in rat thymocytes. Toxicol Appl Pharmacol 169:185–190
15. Philbert MA, Billingsley ML, Reuhl KR 2000 Mechanisms of injury in the central nervous system. Toxicol Pathol 28:43–53
16. Mu YM, Yanase T, Nishi Y, Waseda N, Oda T, Tanaka A, Takayanagi R, Nawata H 2000 Insulin sensitizer, troglitazone, directly inhibits aromatase activity in human ovarian granulosa cells. Biochem Biophys Res Commun 271:710–713
17. Mu YM, Yanase T, Nishi Y, Takayanagi R, Goto K, Nawata H 2001 Combined treatment with specific ligands for PPARγ:RXR nuclear receptor system markedly inhibits the expression of cytochrome P450arom in human granulosa cancer cells. Mol Cell Endocrinol 181:239–248
18. Saitoh M, Yanase T, Morinaga H, Tanabe M, Mu YM, Nishi Y, Nomura M, Okabe T, Goto K, Takayanagi R, Nawata H 2001 Tributyltin or triphenyltin inhibits aromatase activity in the human granulosa-like tumor cell line KGN. Biochem Biophys Res Commun 289:198–204
19. Nishikawa J, Mamiya S, Kanayama T, Nishikawa T, Shiraishi F, Horiguchi T 2004 Involvement of the retinoid X receptor in the development of imposex caused by organotins in gastropods. Environ Sci Technol 38: 6271–6276
20. Baillie-Hamilton PF 2002 Chemical toxins: a hypothesis to explain the global obesity epidemic. J Altern Complement Med 8:185–192
21. Heindel JJ 2003 Endocrine disruptors and the obesity epidemic. Toxicol Sci 76:247–249
22. Jacobs MN, Lewis DF 2002 Steroid hormone receptors and dietary ligands: a selected review. Proc Nutr Soc 61:105–122
23. Watanabe H, Iguchi T, Morohashi K 2002 [Endocrine disruptors and nuclear receptors]. Nippon Rinsho 60: 397–403
24. Kanayama T, Kobayashi N, Mamiya S, Nakanishi T, Nishikawa J 2005 Organotin compounds promote adipocyte differentiation as agonists of the peroxisome proliferator-activated receptor γ/retinoid X receptor pathway. Mol Pharmacol 67:766–774
25. Wang Z, Benoit G, Liu J, Prasad S, Aarnisalo P, Liu X, Xu H, Walker NP, Perlmann T 2003 Structure and function of Nurr1 identifies a class of ligand-independent nuclear receptors. Nature 423:555–560
26. Aarnisalo P, Kim CH, Lee JW, Perlmann T 2002 Defining requirements for heterodimerization between the retinoid X receptor and the orphan nuclear receptor Nurr1. J Biol Chem 277:35118–35123
27. Boehm MF, Zhang L, Zhi L, McClurg MR, Berger E, Wagoner M, Mais DE, Suto CM, Davies JA, Heyman RA, Nadzant AM 1995 Design and synthesis of potent retinoid X receptor selective ligands that induce apoptosis in leukemia cells. J Med Chem 38:3146–3155
28. Yu C, Chen L, Luo H, Chen J, Cheng F, Gui C, Zhang R, Shen J, Chen K, Jiang H, Shen X 2004 Binding analyses between human PPARγ-LBD and ligands. Eur J Biochem 271:386–397
29. Forman BM, Tontonoz P, Chen J, Brun RP, Spiegelman BM, Evans RM 1995 15-Deoxy-δ 12, 14-prostaglandin J2 is a ligand for the adipocyte determination factor PPAR γ. Cell 83:803–812
30. Schoonjans K, Staels B, Auwerx J 1996 The peroxisome proliferator activated receptors (PPARs) and their effects on lipid metabolism and adipocyte differentiation. Biochim Biophys Acta 1302:93–109
31. Kersten S 2002 Peroxisome proliferator activated receptors and obesity. Eur J Pharmacol 440:223–234
32. Lane MD, Tang QQ, Jiang MS 1999 Role of the CCAAT enhancer binding proteins (C/EBPs) in adipocyte differentiation. Biochem Biophys Res Commun 266:677–683
33. Tang QQ, Otto TC, Lane MD 2003 CCAAT/enhancer-binding protein β is required for mitotic clonal expansion during adipogenesis. Proc Natl Acad Sci USA 100: 850–855
34. Tang QQ, Lane MD 1999 Activation and centromeric localization of CCAAT/enhancer-binding proteins during the mitotic clonal expansion of adipocyte differentiation. Genes Dev 13:2231–2241
35. Rubin CS, Hirsch A, Fung C, Rosen OM 1978 Development of hormone receptors and hormonal responsiveness in vitro. Insulin receptors and insulin sensitivity in the preadipocyte and adipocyte forms of 3T3–L1 cells. J Biol Chem 253:7570–7578
36. Kletzien RF, Clarke SD, Ulrich RG 1992 Enhancement of adipocyte differentiation by an insulin-sensitizing agent. Mol Pharmacol 41:393–398
37. Kletzien RF, Foellmi LA, Harris PK, Wyse BM, Clarke SD 1992 Adipocyte fatty acid-binding protein: regulation of gene expression in vivo and in vitro by an insulin-sensitizing agent. Mol Pharmacol 42:558–562
38. Tafuri SR 1996 Troglitazone enhances differentiation, basal glucose uptake, and Glut1 protein levels in 3T3–L1 adipocytes. Endocrinology 137:4706–4712
39. Xue JC, Schwarz EJ, Chawla A, Lazar MA 1996 Distinct stages in adipogenesis revealed by retinoid inhibition of differentiation after induction of PPARγ. Mol Cell Biol 16:1567–1575
40. Kawada T, Kamei Y, Sugimoto E 1996 The possibility of active form of vitamins A and D as suppressors on adipocyte development via ligand-dependent transcriptional regulators. Int J Obes Relat Metab Disord 20(Suppl 3):S52–S57
41. Kawada T, Kamei Y, Fujita A, Hida Y, Takahashi N, Sugimoto E, Fushiki T 2000 Carotenoids and retinoids as suppressors on adipocyte differentiation via nuclear receptors. Biofactors 13:103–109
42. Tontonoz P, Graves RA, Budavari AI, Erdjument-Bromage H, Lui M, Hu E, Tempst P, Spiegelman BM 1994 Adipocyte-specific transcription factor ARF6 is a heterodimeric complex of two nuclear hormone receptors, PPAR γ and RXR α. Nucleic Acids Res 22:5628–5634
43. Martin G, Schoonjans K, Lefebvre AM, Staels B, Auwerx J 1997 Coordinate regulation of the expression of the fatty acid transport protein and acyl-CoA synthetase genes by PPARα and PPARγ activators. J Biol Chem 272:28210–28217
44. Motojima K, Passilly P, Peters JM, Gonzalez FJ, Latruffe N 1998 Expression of putative fatty acid transporter genes are regulated by peroxisome proliferator-activated receptor α and γ activators in a tissue- and inducer-specific manner. J Biol Chem 273:16710–16714
45. Frohnert BI, Hui TY, Bernlohr DA 1999 Identification of a functional peroxisome proliferator-responsive element in the murine fatty acid transport protein gene. J Biol Chem 274:3970–3977
46. Martin G, Poirier H, Hennuyer N, Crombie D, Fruchart JC, Heyman RA, Besnard P, Auwerx J 2000 Induction of the fatty acid transport protein 1 and acyl-CoA synthase

genes by dimer-selective rexinoids suggests that the peroxisome proliferator-activated receptor-retinoid X receptor heterodimer is their molecular target. J Biol Chem 275:12612–12618
47. Tontonoz P, Hu E, Devine J, Beale EG, Spiegelman BM 1995 PPAR γ 2 regulates adipose expression of the phosphoenolpyruvate carboxykinase gene. Mol Cell Biol 15:351–357
48. Magana MM, Lin SS, Dooley KA, Osborne TF 1997 Sterol regulation of acetyl coenzyme A carboxylase promoter requires two interdependent binding sites for sterol regulatory element binding proteins. J Lipid Res 38: 1630–1638
49. Schadinger SE, Bucher NL, Schreiber BM, Farmer SR 2005 PPARγ2 regulates lipogenesis and lipid accumulation in steatotic hepatocytes. Am J Physiol Endocrinol Metab 288:E1195–E1205
50. Tontonoz P, Kim JB, Graves RA, Spiegelman BM 1993 ADD1: a novel helix-loop-helix transcription factor associated with adipocyte determination and differentiation. Mol Cell Biol 13:4753–4759
51. Kim JB, Spiegelman BM 1996 ADD1/SREBP1 promotes adipocyte differentiation and gene expression linked to fatty acid metabolism. Genes Dev 10:1096–1107
52. Joseph SB, Laffitte BA, Patel PH, Watson MA, Matsukuma KE, Walczak R, Collins JL, Osborne TF, Tontonoz P 2002 Direct and indirect mechanisms for regulation of fatty acid synthase gene expression by liver X receptors. J Biol Chem 277:11019–11025
53. Seo JB, Moon HM, Kim WS, Lee YS, Jeong HW, Yoo EJ, Ham J, Kang H, Park MG, Steffensen KR, Stulnig TM, Gustafsson JA, Park SD, Kim JB 2004 Activated liver X receptors stimulate adipocyte differentiation through induction of peroxisome proliferator-activated receptor γ expression. Mol Cell Biol 24:3430–3444
54. Yu S, Matsusue K, Kashireddy P, Cao WQ, Yeldandi V, Yeldandi AV, Rao MS, Gonzalez FJ, Reddy JK 2003 Adipocyte-specific gene expression and adipogenic steatosis in the mouse liver due to peroxisome proliferator-activated receptor γ1 (PPARγ1) overexpression. J Biol Chem 278:498–505
55. Hallakou S, Doare L, Foufelle F, Kergoat M, Guerre-Millo M, Berthault MF, Dugail I, Morin J, Auwerx J, Ferre P 1997 Pioglitazone induces in vivo adipocyte differentiation in the obese Zucker fa/fa rat. Diabetes 46:1393–1399
56. de Souza CJ, Eckhardt M, Gagen K, Dong M, Chen W, Laurent D, Burkey BF 2001 Effects of pioglitazone on adipose tissue remodeling within the setting of obesity and insulin resistance. Diabetes 50:1863–1871
57. Smith SR, De Jonge L, Volaufova J, Li Y, Xie H, Bray GA 2005 Effect of pioglitazone on body composition and energy expenditure: a randomized controlled trial. Metabolism 54:24–32
58. Auwerx J 1999 PPARγ, the ultimate thrifty gene. Diabetologia 42:1033–1049
59. Ferre P 2004 The biology of peroxisome proliferator-activated receptors: relationship with lipid metabolism and insulin sensitivity. Diabetes 53(Suppl 1):S43–S50
60. Day C 1999 Thiazolidinediones: a new class of antidiabetic drugs. Diabet Med 16:179–192
61. Mukherjee R, Davies PJ, Crombie DL, Bischoff ED, Cesario RM, Jow L, Hamann LG, Boehm MF, Mondon CE, Nadzan AM, Paterniti Jr JR, Heyman RA 1997 Sensitization of diabetic and obese mice to insulin by retinoid X receptor agonists. Nature 386:407–410
62. Hill JO, Peters JC 1998 Environmental contributions to the obesity epidemic. Science 280:1371–1374
63. Barker DJ, Bull AR, Osmond C, Simmonds SJ 1990 Fetal and placental size and risk of hypertension in adult life. Br Med J 301:259–262
64. Phillips DI, Hirst S, Clark PM, Hales CN, Osmond C 1994 Fetal growth and insulin secretion in adult life. Diabetologia 37:592–596
65. Martyn CN, Barker DJ, Jespersen S, Greenwald S, Osmond C, Berry C 1995 Growth in utero, adult blood pressure, and arterial compliance. Br Heart J 73:116–121
66. Yajnik C 2000 Interactions of perturbations in intrauterine growth and growth during childhood on the risk of adult-onset disease. Proc Nutr Soc 59:257–265
67. Barker DJ, Martyn CN, Osmond C, Hales CN, Fall CH 1993 Growth in utero and serum cholesterol concentrations in adult life. Br Med J 307:1524–1527
68. Lucas A 1998 Programming by early nutrition: an experimental approach. J Nutr 128:401S–406S
69. Armitage JA, Khan IY, Taylor PD, Nathanielsz PW, Poston L 2004 Developmental programming of metabolic syndrome by maternal nutritional imbalance; how strong is the evidence from experimental models in mammals? J Physiol 561:355–377
70. Masuno H, Kidani T, Sekiya K, Sakayama K, Shiosaka T, Yamamoto H, Honda K 2002 Bisphenol A in combination with insulin can accelerate the conversion of 3T3-L1 fibroblasts to adipocytes. J Lipid Res 43:676–684
71. Masuno H, Okamoto S, Iwanami J, Honda K, Shiosaka T, Kidani T, Sakayama K, Yamamoto H 2003 Effect of 4-nonylphenol on cell proliferation and adipocyte formation in cultures of fully differentiated 3T3-L1 cells. Toxicol Sci 75:314–320
72. Toschke AM, Koletzko B, Slikker Jr W, Hermann M, von Kries R 2002 Childhood obesity is associated with maternal smoking in pregnancy. Eur J Pediatr 161:445–448
73. von Kries R, Toschke AM, Koletzko B, Slikker Jr W 2002 Maternal smoking during pregnancy and childhood obesity. Am J Epidemiol 156:954–961
74. Oken E, Huh SY, Taveras EM, Rich-Edwards JW, Gillman MW 2005 Associations of maternal prenatal smoking with child adiposity and blood pressure. Obes Res 13: 2021–2028
75. Power C, Jefferis BJ 2002 Fetal environment and subsequent obesity: a study of maternal smoking. Int J Epidemiol 31:413–419
76. Hill SY, Shen S, Locke Wellman J, Rickin E, Lowers L 2005 Offspring from families at high risk for alcohol dependence: increased body mass index in association with prenatal exposure to cigarettes but not alcohol. Psychiatry Res 135:203–216
77. Umesono K, Murakami KK, Thompson CC, Evans RM 1991 Direct repeats as selective response elements for the thyroid hormone, retinoic acid, and vitamin D3 receptors. Cell 65:1255–1266
78. Perlmann T, Rangarajan PN, Umesono K, Evans RM 1993 Determinants for selective RAR and TR recognition of direct repeat HREs. Genes Dev 7:1411–1422
79. Blumberg B, Mangelsdorf DJ, Dyck JA, Bittner DA, Evans RM, De Robertis EM 1992 Multiple retinoid-responsive receptors in a single cell: families of retinoid "X" receptors and retinoic acid receptors in the *Xenopus* egg. Proc Natl Acad Sci USA 89:2321–2325
80. Blumberg B, Bolado J Jr., Derguini F, Craig AG, Moreno TA, Chakravarti D, Heyman RA, Buck J, Evans RM 1996 Novel retinoic acid receptor ligands in *Xenopus* embryos. Proc Natl Acad Sci USA 93:4873–4878
81. Blumberg B, Sabbagh Jr W, Juguilon H, Bolado Jr J, van Meter CM, Ong ES, Evans RM 1998 SXR, a novel steroid and xenobiotic-sensing nuclear receptor. Genes Dev 12: 3195–3205
82. Tabb MM, Sun A, Zhou C, Grun F, Errandi J, Romero K, Pham H, Inoue S, Mallick S, Lin M, Forman BM, Blumberg B 2003 Vitamin K2 regulation of bone homeostasis is mediated by the steroid and xenobiotic receptor SXR. J Biol Chem 278:43919–43927
83. Grun F, Blumberg B 2003 Identification of novel nuclear hormone receptor ligands by activity-guided purification. Methods Enzymol 364:3–24
84. Grun F, Venkatesan RN, Tabb MM, Zhou C, Cao J, Hemmati D, Blumberg B 2002 Benzoate X receptors α

and β are pharmacologically distinct and do not function as xenobiotic receptors. J Biol Chem 277:43691–43697
85. Livak KJ, Schmittgen TD 2001 Analysis of relative gene expression data using real-time quantitative PCR and the 2(-Δ Δ C(T)) method. Methods 25:402–408
86. Bourguet W, Ruff M, Chambon P, Gronemeyer H, Moras D 1995 Crystal structure of the ligand-binding domain of the human nuclear receptor RXR-α. Nature 375:377–382
87. Allegretto EA, McClurg MR, Lazarchik SB, Clemm DL, Kerner SA, Elgort MG, Boehm MF, White SK, Pike JW, Heyman RA 1993 Transactivation properties of retinoic acid and retinoid X receptors in mammalian cells and yeast. Correlation with hormone binding and effects of metabolism. J Biol Chem 268:26625–26633
88. Lehmann JM, Moore LB, Smith-Oliver TA, Wilkison WO, Willson TM, Kliewer SA 1995 An antidiabetic thiazolidinedione is a high affinity ligand for peroxisome proliferator-activated receptor γ (PPAR γ). J Biol Chem 270: 12953–12956
89. Nieuwkoop P, Faber J 1994 Normal table of *Xenopus laevis* (Daudin). 2nd ed. New York: Garland Publishing, Inc.
90. Rugh R 1962 Experimental embryology: techniques and procedures. 3rd ed. Minneapolis: Burgess Publishing Co.

Molecular Endocrinology **is published monthly by The Endocrine Society (http://www.endo-society.org), the foremost professional society serving the endocrine community.**

Tbx6-mediated Notch signaling controls somite-specific *Mesp2* expression

Yukuto Yasuhiko*, Seiki Haraguchi†, Satoshi Kitajima*, Yu Takahashi*, Jun Kanno*, and Yumiko Saga‡§

*Cellular and Molecular Toxicology Division, National Institute of Health Sciences, Kamiyoga 1-18-1, Setagaya-ku, Tokyo 158-8501, Japan; †The Wellcome Trust/Cancer Research UK Gurdon Institute, University of Cambridge, Cambridge CB2 1QN, United Kingdom; and ‡Division of Mammalian Development, National Institute of Genetics, Mishima, Shizuoka 411-8540, Japan

Edited by Kathryn V. Anderson, Sloan-Kettering Institute, New York, NY, and approved January 10, 2006 (received for review September 21, 2005)

Mesp2 is a transcription factor that plays fundamental roles in somitogenesis, and its expression is strictly restricted to the anterior presomitic mesoderm just before segment border formation. The transcriptional on–off cycle is linked to the segmentation clock. In our current study, we show that a T-box transcription factor, Tbx6, is essential for *Mesp2* expression. Tbx6 directly binds to the *Mesp2* gene upstream region and mediates Notch signaling, and subsequent *Mesp2* transcription, in the anterior presomitic mesoderm. Our data therefore reveal that a mechanism, via Tbx6-dependent Notch signaling, acts on the transcriptional regulation of *Mesp2*. This finding uncovers an additional component of the interacting network of various signaling pathways that are involved in somitogenesis.

enhancer | transgenic mouse | RBPJκ | luciferase assay

Somitogenesis not only is an important morphogenic process that generates metameric structures in vertebrates, but it is also a intriguing model system for the study of the interactions among various signaling cascades that facilitate periodic pattern formation. The segmental boundary of each somite forms at the anterior end of the presomitic mesoderm (PSM) or unsegmented paraxial mesoderm, which is supplied from the primitive streak or tailbud at a later stage of development.

Notch signaling plays fundamental roles in segmental pattern formation by means of oscillating the activity in the tailbud, its forward movement through the PSM as traveling waves, and its stabilization at the anterior end of the PSM (1, 2). A segment border forms at the posterior limit of the stabilized stripe of Notch signaling activity (2). The oscillation of the Notch signals in the tailbud region is regulated by the transcription factor Hes7 (3), a glycosyltransferase Lunatic fringe (2), and by Wnt signaling (4). In contrast, the positioning of segment formation by a determination wavefront is thought to be defined by antagonistic interactions between gradients of Fgf signals from the posterior end (5) and retinoic acid (RA) from anterior end of the PSM (6). On the other hand, mutant analyses identified a T-box protein, Tbx6, as an indispensable component for correct PSM differentiation and segmentation (7). However, the direct molecular relationships between these factors have not yet been well characterized.

A basic helix–loop–helix transcription factor, Mesp2, has a crucial role both in somite segment border formation and in the establishment of the rostrocaudal patterning of each somite (8). *Mesp2* shows dynamic and periodical expression in the anterior PSM, which defines the positioning of the forming somite by suppressing Notch signaling, partly through the activation of *lunatic fringe* (2). Genetic analyses have revealed that *Mesp2* expression itself is controlled by Notch signaling, which indicates the presence of a complicated feedback circuitry (9, 10). However, the molecular mechanisms that control *Mesp2* expression remain largely unknown. In our present study, we show that Tbx6 directly binds to upstream elements of the *Mesp2* gene and is essential for the activation of *Mesp2* expression. Furthermore, we demonstrate that Notch signaling strongly enhances *Mesp2* activation by Tbx6, and we identify the sequences that are important for this enhancement. Hence, we identify a Tbx6-mediated Notch signaling pathway as a mechanism underlying the regulation of *Mesp2* expression.

Results and Discussion

Evolutionally Conserved Sites in the Upstream Region of the *Mesp2* Gene Promote Strong Reporter Activity in Forming Somites. The distinct expression patterns of *Mesp2* expression during somitogenesis are strictly regulated. As we previously reported (11), a transgenic approach has revealed that a 300-bp portion of the 5′-adjoining sequence of the *Mesp2* ORF induces lacZ reporter activity in forming somites. This finding reflects the *Mesp2* expression pattern in the anteriormost PSM, suggesting that this 5′ region includes cis elements that regulate PSM-specific *Mesp2* expression. We performed comparisons of the genomic sequences of mouse *Mesp2* and its putative ortholog in zebrafish, *mespb*, and identified five conserved sites (A–E) in this 300-bp segment (Fig. 1*A*). Each of these sites was then independently examined for enhancer properties by using a transgenic strategy. We previously showed that one of our transgenic constructs, *P2L-100*, containing sites D and E, which cover the 100 bp upstream of the *Mesp2* ATG start codon, did not activate the lacZ reporter gene (11). We thus concentrated our analysis on sites A–C in our current experiments by ligating them with the *P2L-100* construct. None of these three sites could individually promote lacZ reporter activity in somites (Fig. 1*B*). However, the combination of sites A and B (designated as "site A+B" hereafter) induced strong β-gal expression in the somite region (Fig. 1*B Left*). This result suggests that specific transcription factors required for somite-specific *Mesp2* expression may bind to site A+B.

Tbx6 Binds to Cis-Regulatory Elements of the *Mesp2* Gene and Activates Its Expression. To identify transcription factors that bind to the cis-regulatory elements of the *Mesp2* gene, we performed yeast one-hybrid screening. Using site A+B sequences as the "bait," we isolated a T-box transcription factor, Tbx6, as a candidate binding protein. T-box proteins have been shown to recognize and bind to nucleotide sequences of 10–11 bp in length that possess a conserved CACAC motif (12). Significantly, sites A, B, and D in the upstream sequences of the *Mesp2* gene contain this motif (Fig. 2*A*). EMSA subsequently revealed that FLAG-Tbx6 binds to both site B and site D, in addition to the T (Brachyury) binding consensus sequence (12) (Fig. 6*A*, which is published as supporting information on the PNAS web site). By using site B sequences as a probe for FLAG-Tbx6 binding, EMSA experiments produced two band shifts, a distinct band

Conflict of interest statement: No conflicts declared.

This paper was submitted directly (Track II) to the PNAS office.

Abbreviations: PSM, presomitic mesoderm; NICD, Notch intracellular domain; RA, retinoic acid.

§To whom correspondence should be addressed. E-mail: ysaga@lab.nig.ac.jp.

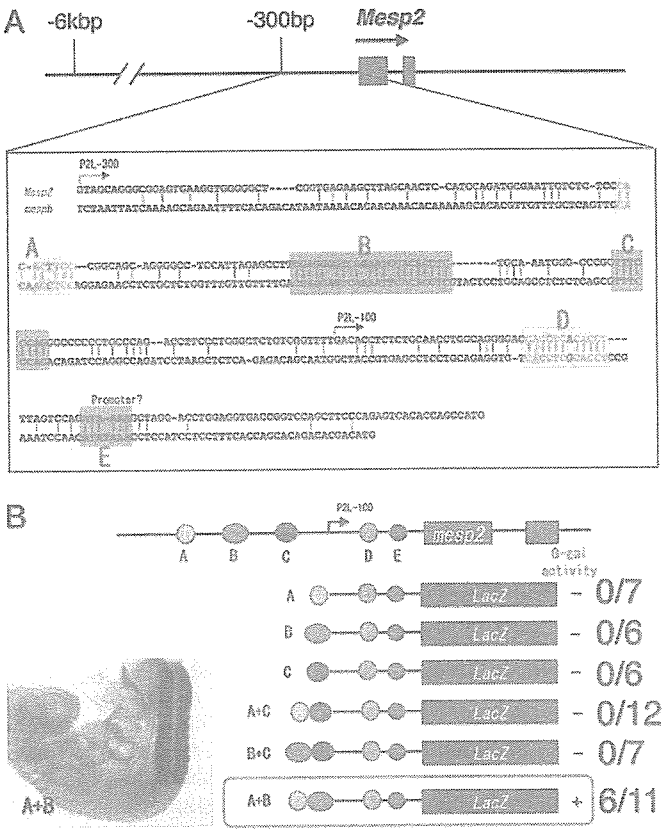

Fig. 1. Characterization of the *Mesp2* enhancer region. (*A*) Comparisons between the genomic sequences of mouse *Mesp2* and zebrafish *mespb* (an ortholog of mouse *Mesp2*) reveal five conserved sites in the 300-bp proximal promoter region. These conserved sites are denoted as A–E. The numbers above the genomic sequences indicate the base count from the ATG transcriptional start site of the *Mesp2* ORF. (*B*) Summary of the transient transgenic assay results with different combinations of conserved sites from the *Mesp2* upstream region (sites A–C). Each site was tested either alone or in combination with other sites for somite-specific enhancer activity. The presence (+) or absence (−) of β-gal activity and the incidence of this among transgene-positive embryos is shown schematically on the right of each reporter construct. The combination of site A and site B (shown as A+B) resulted in strong somite-specific enhancer activity (*Left*).

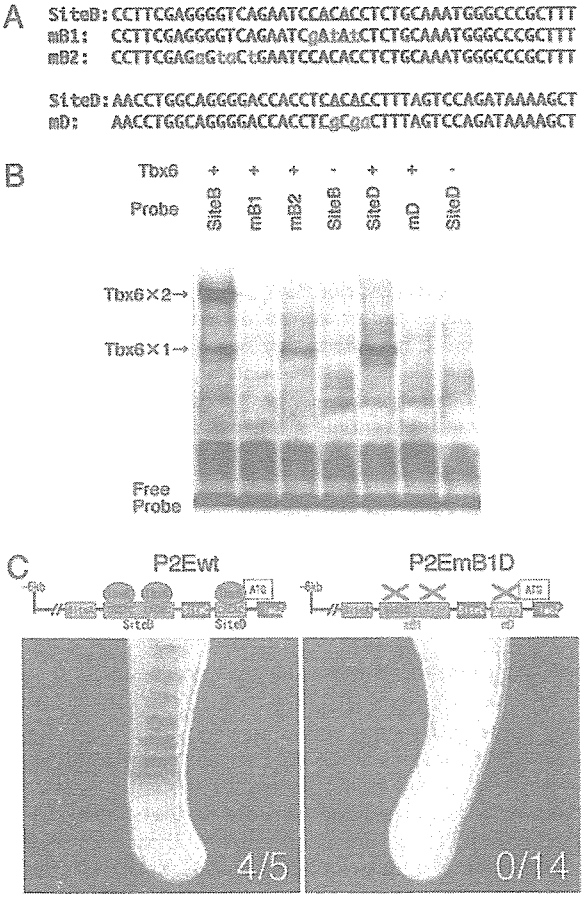

Fig. 2. Tbx6 binds to the *Mesp2* enhancer and promotes gene expression. (*A*) Wild-type and mutant sequences of site B and site D. The bases highlighted in lowercase denote the mutation sites. (*B*) Tbx6 binds to site B and site D. Digoxigenin-labeled oligonucleotide probes containing site B or site D were subjected to EMSA with (+) and without (−) Tbx6. Mutation of the CACAC motif in site B (lane mB1) resulted in the loss of both the wild-type band shifts, whereas mutations in GGGTC (lane mB2) abolished only the upper band. Mutations in the CACAC motif from site D also eliminated the band shift (lane mD). (*C*) β-Gal reporter expression analysis in transgenic mouse embryos with constructs containing either wild-type or mutated *Mesp2* upstream regions. Each of the images is a lateral view with the anterior region toward the top. The numbers of β-gal-positive transgenic embryos are shown in each image (β-gal-positive/transgene-positive).

with a lower mobility and a weaker band with a higher mobility. These two species presumably represent the binding of two and one Tbx6 molecule(s), respectively, because palindromic repeats or spaced tandem repeats of two half fragments of site B generated band shift patterns identical to those of site B (Fig. 6*B*). Tbx6 binding to site B and site D was successfully competed for by oligonucleotides containing the T binding consensus sequence and could be supershifted by incubation of the forming complexes with an anti-FLAG antibody (Fig. 6*A*). We conclude therefore that Tbx6 binds to the upstream region of the *Mesp2* gene by means of the DNA binding activity of its T-box domain.

We next introduced nucleotide substitutions to the conserved CACAC motifs in sites B and D and examined the binding ability of Tbx6 to these mutated oligonucleotide probes. Interestingly, a mutation in site B, designated mB1 (Fig. 2*A*), eliminated both of the wild-type site B band shifts in an EMSA (Fig. 2*B*). Because T-box transcription factors can recognize palindromic sequences and bind to these sites as dimers (13, 14), we introduced nucleotide substitutions to the GGGTC sequence in site B, which is situated in the 5′ region adjacent to the CACAC motif (Fig. 2*A*, mB2). In subsequent EMSA analysis, the mB2 substitution was found to have eliminated only the upper site B band shift, indicating that this mutant oligonucleotide can bind only one Tbx6 molecule (Fig. 2*B*). These results suggest that site B is a partial palindrome that associates with two Tbx6 molecules and that the initial binding depends on the CACAC motif. The site D probe generated one EMSA band, and mutation of the CACAC motif in this site (mD) eliminated this band shift (Fig. 2*B*).

T-box proteins constitute a large family of transcription factors (15). *Tbx18* (16) and *Brachyury* (*Bra*) (17) are expressed in segmented somites and in the tailbud, respectively. Mga is a ubiquitous transcriptional repressor that possesses both T-box and basic helix–loop–helix motifs (18), and the T-box motifs of Mga and Tbx6 show similarities (19). In our present experiments, we examined the DNA-binding abilities of Tbx6, Bra, Mga, and Tbx18 to upstream *Mesp2* sequences using EMSA experiments (Fig. 6*D*). Bra and Tbx18 showed no binding activity to either site B or site D, whereas Mga bound weakly to site B. Taken together, we conclude from these data that Tbx6 is the most likely factor, among the T-box-containing proteins expressed in the PSM, that binds to site B and site D of the *Mesp2* gene.

To examine the function of these upstream *Mesp2* cis elements on gene expression, we performed transient transgenic mouse analyses using a lacZ reporter with mutated cis elements in 6-kb upstream sequences of the *Mesp2* ORF. The nucleotide substitutions that eliminate the binding of Tbx6 to sites B and D of the *Mesp2* promoter (P2EmB1D) diminished gene reporter activity in these assays (Fig. 2*C*). Furthermore, targeted disruption of sites B and D eliminated *Mesp2* expression in the forming somites of homozygous embryos (data not shown), demonstrating that these cis-regulatory elements are essential for somite-specific *Mesp2* expression.

In mouse embryo, *Mesp2* mRNA emerges in anterior PSM, at the position of S-1 (8, 9). Tbx6 protein exists also in S-1 (20). *Mesp2* is not expressed in the PSM of *Tbx6*-null mouse embryos (7), suggesting that it is a downstream target of Tbx6. Although the distinct *Mesp2* signal overlaps only in the anteriormost part of *Tbx6*, the initial *Mesp2* mRNA emerges in the more posterior region, overlapping with the *Tbx6* signal (Fig. 6*E*). These results suggest that Tbx6 is necessary at least for initiation of *Mesp2* expression.

In zebrafish, *fused somite* (*fss*), which encodes *Tbx24*, is known as a distant homolog of mouse *Tbx6*, and the corresponding mutant embryos have neither segmented somite nor *mespb* expression (21). The cis-regulatory elements are also well conserved between the upstream regions of *Mesp2* and *mespb* (Fig. 1*A*), and Tbx24 also binds to the *Mesp2* upstream region (data not shown). Recently, Davidson *et al.* (22) reported that, during heart development in the simple chordate *Ciona intestinalis*, a *Mesp* homolog is also expressed in a Tbx6-dependent manner. Comparing genomic sequences among *Ciona*, mouse, and zebrafish, the authors identified multiple Tbx6 binding sites in the upstream sequence of *Ciona Mesp* homolog. Taken together, we speculate from these findings that Tbx6-mediated activation of the *Mesp* genes is an evolutionally conserved mechanism in Chordata.

The Notch Intracellular Domain (NICD) Activates a *Mesp2* Reporter Construct in a Tbx6-Dependent Manner. To analyze the detailed regulatory mechanisms underlying the control of *Mesp2* expression, we constructed a *Mesp2* reporter system comprising a firefly luciferase reporter and *Mesp2* cis elements. Cotransfection of a Tbx6 expression vector with the *Mesp2* reporter increased luciferase activity by 10-fold (Fig. 3), indicating that Tbx6 functions as a transcriptional activator of *Mesp2*. In somite-stage embryos, *Tbx6* is expressed throughout the PSM and also in the tailbud region (20, 23), whereas *Mesp2* expression is restricted to the anterior PSM just before somite formation, and the expression overlaps only in the anterior limit of the *Tbx6* expression domain (Fig. 6*E*). The discrepancy between these expression patterns strongly indicates that other unknown factor(s) participate in the pathways that restrict the *Mesp2* expression domain to the anterior PSM. Because Notch signaling plays crucial roles in many aspects of somitogenesis, and given that *Mesp2* expression is known to depend on Dll1-Notch signaling (10), we examined the involvement of Notch signaling in the Tbx6-mediated transactivation of *Mesp2*.

The typical Notch signaling pathway is composed of ligands known as DSL (Delta, Serrate, and Lag-2), Notch receptors, effectors known as CSL (CBF-1, Suppressor of Hairless, and Lag-1), and a number of other proteins that modulate the functions of each component of the pathway (24). Once the DSL ligands bind to the Notch receptor, the NICD is proteolytically cleaved, translocates into the nucleus, and binds to its CSL effector (RBPJκ in the case of mouse) to activate the transcription of downstream target genes (24). We transiently introduced expression vectors for NICD and RBPJκ-VP16 (dominant-active RBPJκ) (25), in conjunction with Tbx6, into cultured cells bearing the *Mesp2* reporter. As a positive control, we used the

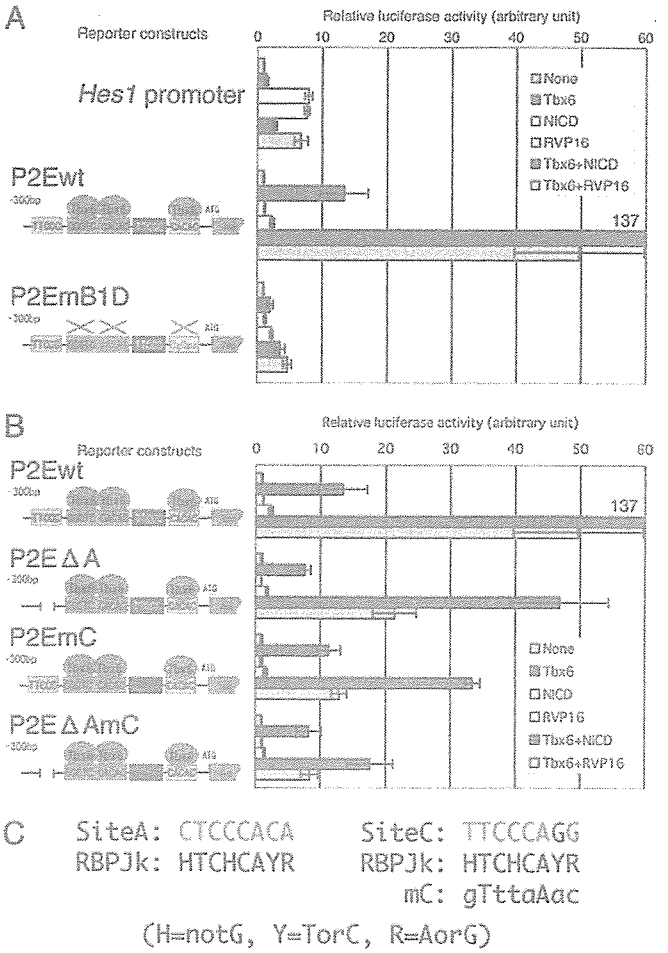

Fig. 3. *Mesp2* expression is activated by Notch signaling in a Tbx6-dependent manner. For each set of analyses, the luciferase activity was normalized to the values obtained in the absence of an expression vector (None). Error bars represent the standard deviation from six independent experiments. RVP16, RBPJκ-VP16. (*A*) Tbx6 activates a *Mesp2*–luciferase reporter gene construct synergistically with the NICD or RBPJκ-VP16. Mutation of site B and site D (denoted as P2EmB1D) eliminates this transactivation. (*B*) Notch signal activates the *Mesp2* reporter construct via site A and site C. The reporter constructs are indicated to the left of the graph. (*C*) Nucleotide sequences of the possible RBPJκ binding sites in site A (*Left*) and site C (*Right*) and the comparison between these regions and the RBPJκ binding consensus sequence (denoted as RBPJk) (27). The nucleotides matching the consensus sequence are shown in red for site A and site C. Nucleotide substitutions in site C (denoted as mC) are indicated in lowercase.

Hes1 promoter, which is known to be a downstream target of Notch signaling (26). Transfection of the *Hes1* reporter construct produced significant luciferase activity even in the absence of NICD (data not shown), reflecting the endogenous NICD activity, and the reporter activity increased further in the presence of either NICD or RBPJκ-VP16. In contrast, neither NICD nor RBPJκ-VP16 was found to activate the *Mesp2* reporter (Fig. 3*A*). However, when NICD and Tbx6 were cotransfected, significant increases in luciferase activity were detected (Fig. 3*A*). RBPJκ-VP16 also can activate the *Mesp2* promoter when cotransfected with *Tbx6* (Fig. 3*A*), suggesting that RBPJκ-dependent Notch signaling activated *Mesp2* reporter in a Tbx6-dependent manner. Consistent with this finding, mutations in site B and site D, which eliminate Tbx6 binding to the *Mesp2* upstream region, greatly reduced *Mesp2* reporter activation by NICD or RBPJκ-VP16 (Fig. 3*A*).

To identify the Notch signaling responsive site within the

Mesp2 upstream region, we analyzed the activity of two additional reporter constructs bearing either a deletion or a mutation in the conserved sites A and C, because these regions contain sequences that have some similarity to the RBPJκ consensus binding site (24, 27) (Fig. 3*C*). We speculated that these sites may play an important role in the regulation of *Mesp2* expression based on our observation that site A is essential for somite-specific expression in combination with site B (Fig. 1). Moreover, reporter activity in forming somites is lost when sequential deletion of the upstream region of the *Mesp2* gene removes a part of site C (11). In our current experiments, the deletion of site A reduced the levels of synergistic activation of the *Mesp2* reporter by both Notch signaling and Tbx6 by up to 50% (Fig. 3*B*, P2EΔA). Reporter activation was also remarkably diminished when we introduced mutations into both site A and site C (Fig. 3*B*, P2EΔAmC), suggesting that the binding of RBPJκ is required for the Tbx6-dependent transduction of Notch signaling. In contrast to the *Hes* family genes, no direct interaction between the Notch signaling pathway and the *Mesp2* regulatory region had been previously identified. Our current findings thus provide the first evidence that *Mesp2* is a direct target of Notch signaling. Furthermore, we identified a regulatory mechanism underlying the Notch signaling pathway that is based on the binding of Tbx6 to transcriptional regulatory sequences (summarized in Fig. 4 *A* and *B*).

We next conducted transient transgenic assays using our lacZ reporters with mutations in sites A and C. Surprisingly, the coexistence of the site A deletion and site C mutation (P2EΔAmC) in our reporter system showed somite-specific β-gal expression, although the activity was slightly weaker than normal (Fig. 5*A*). One possibility that might explain this disparity is that there may be a redundant, RBPJκ-independent pathway of Notch signaling that activates *Mesp2* expression. Consistent with this hypothesis, the P2EΔAmC reporter retained the ability to respond to the coexpression of NICD and Tbx6, although this activity was only 13% of wild-type levels (Fig. 3*B*). Notably, the P2EΔAmC reporter showed no synergistic activation after the coexpression of Tbx6 and RBPJκ-VP16 (Fig. 3*B*), indicating that the ability to respond to RBPJκ-dependent Notch signaling is eliminated by the disruption of sites A and C. These results suggest that Notch signaling activates *Mesp2* expression in both RBPJκ-dependent and RBPJκ-independent manners (Fig. 4*C*). Although most of the Notch signals are mediated by CSL effectors, such as RBPJκ, there is some reported evidence that suggests the existence of RBPJκ-independent Notch signal transduction pathways (28, 29). The molecular components involved in RBPJκ-independent Notch signaling are still poorly understood, but our present data suggest the possibility that Tbx6 not only facilitates RBPJκ-dependent Notch signaling but also acts as a component of an RBPJκ-independent Notch signaling pathway.

Another possible mechanism of somite-specific reporter expression that we observed in our P2EΔAmC transgenic embryos is the involvement of Notch-independent signals (Fig. 4*C*). Although it is clear that Notch signaling is genetically upstream of *Mesp2* activation (9, 10), *Psen1* knockout mouse embryos, which are deficient in Notch proteolysis and therefore do not produce NICD (30), show only moderate decreases in *Mesp2* expression levels (10). Together with our present findings, these observations may indicate that the controlling mechanism for *Mesp2* gene expression is a redundant and robust system and is composed of a number of signaling cascades. Regardless of this possibility, Tbx6 is likely to be essential for all of the signaling pathways involved in *Mesp2* expression, because mutation of the Tbx6 binding sites in the upstream regions of the *Mesp2* gene completely eliminates reporter expression in forming somites (Fig. 2*C*).

Because Tbx6 mRNA (Fig. 6*E*) and protein (20) are distributed throughout the tailbud and posterior PSM, the factors that restrict the expression domain of *Mesp2* in anterior PSM remain to be identified. Notably, although Tbx6 seems to activate reporter expression in cultured cells by itself, dominant-negative RBPJκ(R218H), which retains NICD binding activity but has lost any DNA binding ability (31), inhibits the Tbx6-dependent reporter activation by 50% (Fig. 5*B*). This finding suggests that

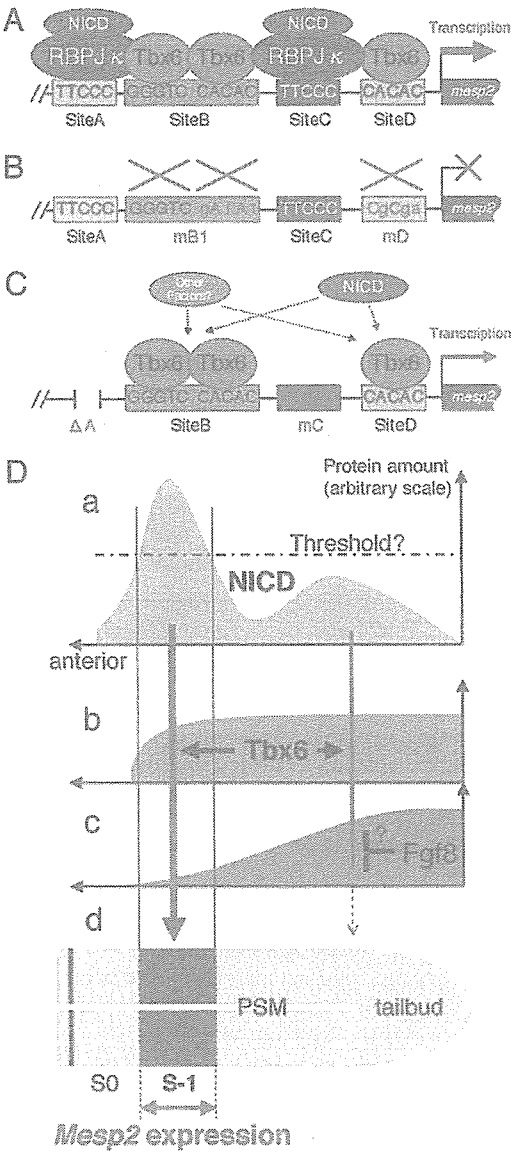

Fig. 4. Proposed mechanisms underlying the control of *Mesp2* expression. Tbx6 and NICD (colored ovals) interact with the conserved upstream sites in the *Mesp2* gene, sites A–D (represented by boxes). Tbx6 binds to site B (two molecules) and site D (single molecule). Site A and site C interact with RBPJκ to achieve a significant increase in *Mesp2* expression levels in the presence of Notch signals (*A*). This activation fully depends on the binding of Tbx6 to site B or site D (*B*). Tbx6 may activate *Mesp2* expression without site A and site C, presumably through an RBPJκ-independent Notch signaling pathway and via other signals (*C*). (*D*) Schematic representation of a proposed model that may explain developmentally regulated *Mesp2* expression in the anterior PSM. (*a*) NICD is highly accumulated in the anterior PSM and less in the posterior (1, 2) to activate *Mesp2* expression (red arrows). There may be a threshold level of NICD accumulation to initiate *Mesp2* activation (broken line). (*b*) Tbx6 protein is distributed in the tailbud and PSM (20) and facilitates *Mesp2* activation by NICD. (*c*) It is possible that the activation of *Mesp2* expression in the tailbud and posterior PSM, if any, is repressed by other factor(s), such as Fgf8 (36), via an unknown mechanism. (*d*) As a result, *Mesp2* expression is restricted in the anterior PSM (red box).

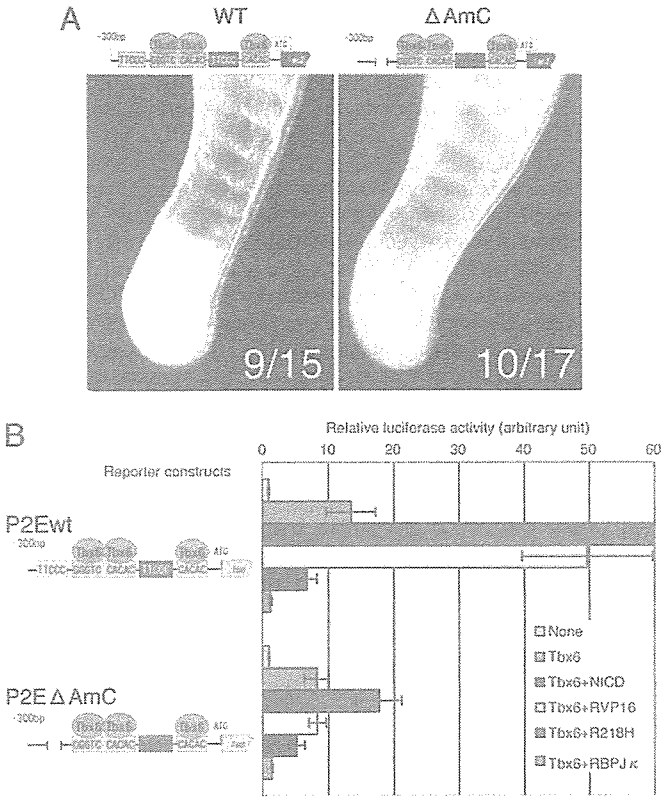

Fig. 5. The expression of *Mesp2* is not achieved solely by RBPJκ-dependent Notch signaling. (*A*) Transgenic analyses reveal that somite-specific reporter expression can still be observed by using the P2EΔAmC construct, which contains a deletion of site A and mutations in site C. The numbers of β-gal-positive embryos are indicated for each image (β-gal-positive/transgene-positive). (*B*) The expression of a dominant-negative RBPJκ diminishes reporter activation by Tbx6 for both the wild-type (wt) and P2EΔAmC (Tbx6+R218H, purple bars) vectors. Wild-type RBPJκ also strongly suppressed reporter activity driven by Tbx6 (Tbx6+RBPJκ, orange bars). Error bars represent the standard deviation in six independent experiments.

Tbx6 itself has only weak transactivation properties, if any, and needs to cooperate with other signals such as Notch for full activity. We speculate that reporter activation by Tbx6 itself (Figs. 3 and 5) may be accomplished by cooperation with Notch signaling, presumably driven by endogenous NICD in cultured cells. Endogenous NICD concentration in cells or tissues is very low and biochemically undetectable (32). However, cultured fibroblast cells express mature Notch protein (33) and show γ-secretase-like activity that generates NICD from Notch protein (32). Furthermore, NICD activates *Hes1* reporter at very low concentrations, below the level of biochemical detection (32). Consistent with these data, *Hes1* reporter showed higher basal activity than *Mesp2* reporters or control reporter with no promoter/enhancer: 100 times higher in COS-7 cells and 60 times higher in NIH/3T3 cells in our observation (data not shown). We suppose that endogenous NICD affects the expression of Notch downstream genes in cultured cells.

NICD accumulation is observed as a strong band-like pattern in the anterior PSM and as a weak diffused signal in the posterior PSM (1, 2). Mesp2 is initially detectable in the middle of a distinct band of NICD in the anterior PSM (2), consistent with the importance of Notch signaling in *Mesp2* expression indicated by our present study. However, the weak Notch signaling activity observed in the posterior PSM may activate *Mesp2* expression, whereas *Mesp2* transcripts appear only in the anterior PSM. One possibility is that there is a "threshold" of NICD levels that is required to trigger Tbx6-dependent *Mesp2* activation (Fig. 4*D*). Because RBPJκ is expressed ubiquitously in the developing embryo (34) and strongly represses Tbx6-dependent activation of the *Mesp2* reporters (Fig. 5*B*), it may also function as a suppressor in the posterior PSM that prevents inadequate expression of *Mesp2*.

Recent reports also indicate that there are two gradients of mutually inhibitory signals, Fgf8 and RA, that have important roles in the positional determination of segment formation (35). It is likely therefore that the Fgf8 and RA signals also participate in the regulation of *Mesp2* expression. Recently, Delfini *et al.* (36) reported an intriguing result suggesting that Fgf signaling represses *Mesp* expression. Using *in ovo* electroporation, they demonstrated that the up-regulation of Fgf in the PSM diminishes the endogenous expression of *cMeso*, the chick *Mesp* homolog. It is plausible therefore that Fgf8, which is strongly expressed in the tailbud and posterior PSM, prevents the inadequate expression of *Mesp2* in posterior region. The involvement of RA in *Mesp2* expression remains elusive, however, because the disruption of *CYP26* (37), a degradation enzyme for RA, does not severely affect *Mesp2* expression levels (2). In the zebrafish embryo, FGF signaling up-regulates a basic helix–loop–helix transcription factor, her13.2, which maintains the oscillation of the Notch signals in both the tailbud and PSM by repressing the Notch-regulated genes *her1* and *her7* (38). RA and Fgf signals may thus contribute to the positioning of *Mesp2* expression by coordinating the regular oscillation of Notch signals in the tailbud and PSM.

Interestingly, it has been revealed that *Tbx6* is one of the direct targets of RBPJκ-dependent Notch signaling (39). During somitogenesis, Notch signals may first activate *Tbx6* expression in the tailbud and posterior PSM region and then activate *Mesp2* expression in the anterior PSM in cooperation with Tbx6. Furthermore, Tbx6 also works upstream of the Notch signaling pathway. In embryos of *Tbx6* hypomorphic mutant mice, *Dll1* expression in the tailbud and posterior PSM is greatly reduced (40). Promoter analyses of *Dll1* have demonstrated that Tbx6, in synergy with Wnt signaling, activates *Dll1* expression by binding to T-binding consensus sequences (20, 41). Taken together, our present results demonstrate that Tbx6 and Notch signaling constitute a regulatory network that controls somite formation via the regulation of *Mesp2* expression.

Materials and Methods

Transgenic Analyses. DNA fragments, with and without mutations in conserved upstream sites, were generated from a *Mesp2* genomic fragment by using a standard PCR-based protocol. Transgene inserts were digested from the corresponding plasmids, purified, and injected into the male pronucleus of a fertilized egg (42). The injected embryos were then transferred into pseudopregnant recipients and allowed to develop until 9.5–10.5 days postcoitum. Embryos were then analyzed for lacZ expression by X-gal staining (43) and subsequently examined for the presence of the transgene by PCR analysis (44).

Yeast One-Hybrid Screening. Synthetic oligonucleotides corresponding to contiguous sequences of conserved site A (nucleotides −199 to −191 from first ATG of *Mesp2* ORF) and site B (nucleotides −162 to −140) were inserted into the vectors pHISi-1 and placZi (Clontech), immediately upstream of the HIS3 and lacZ reporter genes, respectively. The resulting constructs were then linearized and introduced simultaneously into *Saccharomyces cerevisiae* YM4271 (Clontech) to generate the bait strain. The bait strain was then transformed by using 80 μg of 11.5 days postcoitum mouse tail cDNA library plasmid (45) to screen up to 2 million independent clones. We obtained hundreds of positive clones (HIS3+ and LacZ+) and recovered

library plasmid from 77 of these. Fifty-one of these 77 clones were sequenced and found to encode Tbx6.

EMSA. The full-length Tbx6 ORF was obtained from the pACT-Tbx6 construct, which was isolated from the yeast one-hybrid screening. After ligation to a 3XFLAG tag (Sigma), the tagged Tbx6 insert was cloned into pCS2+ (46). *In vitro* transcription/translation was then performed with a TNT *in vitro* translation kit (Promega) following the manufacturer's protocol. Oligonucleotide probes were labeled with digoxigenin-11-dideoxy UTP by using recombinant TdT (Roche Diagnostics). Crude *in vitro* translated product (5 μl) was subjected to EMSA as a protein sample. As a negative control, reticulocyte lysate without Tbx6 template was used. EMSA was performed by using the DIG Gel Shift Kit, 2nd Generation (Roche Diagnostics), following the manufacturer's protocol. The band shifts were detected by using LumiImager LAS-1000 (Fuji).

Luciferase Assay. Segments (356 bp) corresponding to the 5′-adjoining sequence of the *Mesp2* ORF, with and without mutations in the conserved binding sites, were subcloned into the pGL3-Basic (Promega) vector to generate luciferase reporter constructs. The expression vectors for the proteins to be assessed were constructed in the same way as that used in the EMSAs described above. COS-7 cells were routinely and regularly passaged in DMEM supplemented with 10% FBS. Cells were seeded at 2.5×10^4 cells per well in 24-well plates, and, after 24 h of cultivation, they were transfected with a total of 350 ng of DNA containing the reporter plasmids and expression vectors for the proteins under analysis (50 ng of each expression vector and 200 ng of reporter construct, adjusted to 350 ng by the addition of empty vector). Twenty-four hours after transfection, the cells were lysed by Passive Lysis Buffer (Promega) and subjected to a luciferase assay by using the Dual Luciferase System (Promega). In all experiments, 5 ng of the sea pansy luciferase expression vector phRL-TK (Promega) was used per well as the internal control. Luciferase activity was normalized to the phRL-TK internal control activity (sea pansy luciferase). The experiments were performed in triplicate for each assay and repeated at least twice.

We are grateful to Tasuku Honjo (Kyoto University, Kyoto) for providing cDNA clones of RBPJκ, RBPJκ-VP16, and dnRBPJκ (R218H) and to Mariko Ikumi, Eriko Ikeno, and Shinobu Watanabe for technical assistance. We also thank Hiroyuki Takeda, Mitsuru Morimoto, and Masayuki Oginuma for helpful discussions and for their comments on the manuscript. This work was supported by the Organized Research Combination System of the Ministry of Education, Culture, Sports, Science, and Technology, Japan.

1. Huppert, S. S., Ilagan, M. X., De Strooper, B. & Kopan, R. (2005) *Dev. Cell* **8,** 677–688.
2. Morimoto, M., Takahashi, Y., Endo, M. & Saga, Y. (2005) *Nature* **435,** 354–359.
3. Bessho, Y., Hirata, H., Masamizu, Y. & Kageyama, R. (2003) *Genes Dev.* **17,** 1451–1456.
4. Aulehla, A., Wehrle, C., Brand-Saberi, B., Kemler, R., Gossler, A., Kanzler, B. & Herrmann, B. G. (2003) *Dev. Cell* **4,** 395–406.
5. Sawada, A., Shinya, M., Jiang, Y. J., Kawakami, A., Kuroiwa, A. & Takeda, H. (2001) *Development* **128,** 4873–4880.
6. Moreno, T. A. & Kintner, C. (2004) *Dev. Cell* **6,** 205–218.
7. Chapman, D. L. & Papaioannou, V. E. (1998) *Nature* **391,** 695–697.
8. Saga, Y., Hata, N., Koseki, H. & Taketo, M. M. (1997) *Genes Dev.* **11,** 1827–1839.
9. Takahashi, Y., Koizumi, K., Takagi, A., Kitajima, S., Inoue, T., Koseki, H. & Saga, Y. (2000) *Nat. Genet.* **25,** 390–396.
10. Takahashi, Y., Inoue, T., Gossler, A. & Saga, Y. (2003) *Development* **130,** 4259–4268.
11. Haraguchi, S., Kitajima, S., Takagi, A., Takeda, H., Inoue, T. & Saga, Y. (2001) *Mech. Dev.* **108,** 59–69.
12. Conlon, F. L., Fairclough, L., Price, B. M., Casey, E. S. & Smith, J. C. (2001) *Development* **128,** 3749–3758.
13. Mitani, Y., Takahashi, H. & Satoh, N. (2001) *Development* **128,** 3717–3728.
14. Muller, C. W. & Herrmann, B. G. (1997) *Nature* **389,** 884–888.
15. Wilson, V. & Conlon, F. L. (2002) *Genome Biol.* **3,** REVIEWS3008.
16. Kraus, F., Haenig, B. & Kispert, A. (2001) *Mech. Dev.* **100,** 83–86.
17. Koseki, H., Wallin, J., Wilting, J., Mizutani, Y., Kispert, A., Ebensperger, C., Herrmann, B. G., Christ, B. & Balling, R. (1993) *Development* **119,** 649–660.
18. Hurlin, P. J., Steingrimsson, E., Copeland, N. G., Jenkins, N. A. & Eisenman, R. N. (1999) *EMBO J.* **18,** 7019–7028.
19. Lardelli, M. (2003) *Dev. Genes Evol.* **213,** 519–522.
20. White, P. H. & Chapman, D. L. (2005) *Genesis* **42,** 193–202.
21. Nikaido, M., Kawakami, A., Sawada, A., Furutani-Seiki, M., Takeda, H. & Araki, K. (2002) *Nat. Genet.* **31,** 195–199.
22. Davidson, B., Shi, W. & Levine, M. (2005) *Development* **132,** 4811–4818.
23. Chapman, D. L., Agulnik, I., Hancock, S., Silver, L. M. & Papaioannou, V. E. (1996) *Dev. Biol.* **180,** 534–542.
24. Mumm, J. S. & Kopan, R. (2000) *Dev. Biol.* **228,** 151–165.
25. Furriols, M. & Bray, S. (2000) *Dev. Biol.* **227,** 520–532.
26. Jarriault, S., Brou, C., Logeat, F., Schroeter, E. H., Kopan, R. & Israel, A. (1995) *Nature* **377,** 355–358.
27. Barolo, S., Walker, R. G., Polyanovsky, A. D., Freschi, G., Keil, T. & Posakony, J. W. (2000) *Cell* **103,** 957–969.
28. Matsuno, K., Go, M. J., Sun, X., Eastman, D. S. & Artavanis-Tsakonas, S. (1997) *Development* **124,** 4265–4273.
29. Hori, K., Fostier, M., Ito, M., Fuwa, T. J., Go, M. J., Okano, H., Baron, M. & Matsuno, K. (2004) *Development* **131,** 5527–5537.
30. Koizumi, K., Nakajima, M., Yuasa, S., Saga, Y., Sakai, T., Kuriyama, T., Shirasawa, T. & Koseki, H. (2001) *Development* **128,** 1391–1402.
31. Kato, H., Taniguchi, Y., Kurooka, H., Minoguchi, S., Sakai, T., Nomura-Okazaki, S., Tamura, K. & Honjo, T. (1997) *Development* **124,** 4133–4141.
32. Schroeter, E. H., Kisslinger, J. A. & Kopan, R. (1998) *Nature* **393,** 382–386.
33. De Strooper, B., Annaert, W., Cupers, P., Saftig, P., Craessaerts, K., Mumm, J. S., Schroeter, E. H., Schrijvers, V., Wolfe, M. S., Ray, W. J., *et al.* (1999) *Nature* **398,** 518–522.
34. Oka, C., Nakano, T., Wakeham, A., de la Pompa, J. L., Mori, C., Sakai, T., Okazaki, S., Kawaichi, M., Shiota, K., Mak, T. W. & Honjo, T. (1995) *Development* **121,** 3291–3301.
35. Dubrulle, J. & Pourquie, O. (2004) *Development* **131,** 5783–5793.
36. Delfini, M. C., Dubrulle, J., Malapert, P., Chal, J. & Pourquie, O. (2005) *Proc. Natl. Acad. Sci. USA* **102,** 11343–11348.
37. Sakai, Y., Meno, C., Fujii, H., Nishino, J., Shiratori, H., Saijoh, Y., Rossant, J. & Hamada, H. (2001) *Genes Dev.* **15,** 213–225.
38. Kawamura, A., Koshida, S., Hijikata, H., Sakaguchi, T., Kondoh, H. & Takada, S. (2005) *Genes Dev.* **19,** 1156–1161.
39. White, P. H., Farkas, D. R. & Chapman, D. L. (2005) *Genesis* **42,** 61–70.
40. White, P. H., Farkas, D. R., McFadden, E. E. & Chapman, D. L. (2003) *Development* **130,** 1681–1690.
41. Hofmann, M., Schuster-Gossler, K., Watabe-Rudolph, M., Aulehla, A., Herrmann, B. G. & Gossler, A. (2004) *Genes Dev.* **18,** 2712–2717.
42. Hogan, B., Beddington, R., Costantini, F. & Lacy, E. (1994) *Manipulating the Mouse Embryo: A Laboratory Manual* (Cold Spring Harbor Lab. Press, Woodbury, NY).
43. Saga, Y., Yagi, T., Ikawa, Y., Sakakura, T. & Aizawa, S. (1992) *Genes Dev.* **6,** 1821–1831.
44. Sasaki, H. & Hogan, B. L. (1996) *Genes Cells* **1,** 59–72.
45. Ohara, O., Nagase, T., Mitsui, G., Kohga, H., Kikuno, R., Hiraoka, S., Takahashi, Y., Kitajima, S., Saga, Y. & Koseki, H. (2002) *DNA Res.* **9,** 47–57.
46. Rupp, R. A., Snider, L. & Weintraub, H. (1994) *Genes Dev.* **8,** 1311–1323.

Journal of Pathology
J Pathol 2006; **209**: 522–531
Published online 25 April 2006 in Wiley InterScience (www.interscience.wiley.com). **DOI:** 10.1002/path.1993

Original Paper

PTOV1: a novel testosterone-induced atherogenic gene in human aorta

Y Nakamura,[1] T Suzuki,[1] K Igarashi,[4] J Kanno,[4] T Furukawa,[2] C Tazawa,[1] F Fujishima,[1] I Miura,[1] T Ando,[4] N Moriyama,[1] T Moriya,[1] H Saito,[5] S Yamada[3] and H Sasano[1]*

[1]*Department of Pathology, Tohoku University School of Medicine, Sendai, Japan*
[2]*Department of Molecular Pathology, Tohoku University School of Medicine, Sendai, Japan*
[3]*Department of Radiology, Tohoku University School of Medicine, Sendai, Japan*
[4]*Division of Toxicology, the Biological Safety Research Centre, National Institute of Health Sciences, Tokyo, Japan*
[5]*Department of Radiology, Sendai Medical Centre, Sendai, Japan*

*Correspondence to: Dr H Sasano, Department of Pathology, Tohoku University School of Medicine, 2-1 Seiryo-machi, Aoba-ku, Sendai, 980-8575 Japan. E-mail: hsasano@patho1a2.med.tohoku.ac.jp

Received: 25 October 2005
Revised: 8 February 2006
Accepted: 4 March 2006

Abstract

There are gender differences in the development of atherosclerosis, possibly owing to differences in sex steroid hormone action and/or metabolism. One of the atherogenic effects of testosterone is thought to be androgen receptor (AR)-mediated vascular smooth muscle cell (VSMC) proliferation. However, the detailed mechanism of this effect, particularly the identity of the genes associated with VSMC proliferation, remains largely unknown. Therefore, we first employed microarray analysis and, subsequently, quantitative RT-PCR to analyse RNA expression in AR-positive human VSMCs treated with testosterone in order to detect testosterone-induced genes associated with cell proliferation. We further examined whether the genes identified were involved in cell proliferation using small interfering RNA (siRNA) transfection. Expression of the gene products was then evaluated in human aorta with various degrees of atherosclerosis in order to evaluate the clinical relevance of the findings. Both microarray and quantitative RT-PCR analyses demonstrated marked induction of the human prostate overexpressed protein 1 (*PTOV1*) gene by testosterone in the cell lines: this gene was recently identified as a novel androgen-induced gene involved in prostate tumour cell proliferation. Inhibition of *PTOV1* by transfection of its corresponding siRNA suppressed testosterone-induced cell proliferation. In human aorta, PTOV1 immunoreactivity in the nuclei of neointimal VSMCs was abundantly detected in male aorta with mild atherosclerotic changes compared with female aorta or male aorta with severe atherosclerotic changes. These findings indicate that the *PTOV1* gene is androgen-responsive in VSMCs and that it may play an important role in androgen-related atherogenesis in the human aorta, particularly early atherosclerosis in the male aorta, through regulating proliferation of neointimal VSMCs.

Keywords: **vascular smooth muscle cells; androgen receptor; testosterone; cell proliferation; PTOV1**

Introduction

There is an important, well-documented, gender difference in coronary heart disease risks, with earlier onset of disease and excess mortality in male subjects [1–3]. Athero-protective effects of oestrogens on vascular structure and function have been proposed as one of the most important mechanisms accounting for this gender difference [4]. On the other hand, an association between androgens and atherosclerosis continues to be disputed. Androgens have been considered to reduce the incidence of ischaemic myocardial disease in men, but they have also been reported to exert atherogenic effects on the human cardiovascular system through promoting plaque formation and enhancing monocyte adhesion to endothelial cells [5–8]. It has been demonstrated that testosterone exerts direct atherogenic effects by promoting cell proliferation through an initial interaction with the androgen receptor (AR) in vascular smooth muscle cells (VSMCs) *in vitro* [9]. However, unlike oestrogens, the possible effects of testosterone on atherogenesis and/or anti-atherogenesis have not been extensively studied. It is therefore important to study the detailed mechanisms of these direct effects of testosterone on the human cardiovascular system.

In this study, we first screened for testosterone-induced genes involved in the proliferation of VSMCs using microarray analysis in cell lines derived from AR-positive human VSMCs. We then confirmed the results by employing other *in vitro* studies. As testosterone induced marked overexpression of *PTOV1* in

these assays, we subsequently examined the levels of expression of PTOV1 protein in VSMCs in samples of the human abdominal aorta obtained at autopsy.

Materials and methods

Vascular smooth muscle cells

Two types of human dedifferentiated VSMCs, ie HUVS-112D (derived from human umbilical cord), and T/G HA-VSMC (derived from human aorta) were commercially obtained from American Type Culture Collection (Manassas, VA, USA) [10,11]. We examined whether these cells expressed AR using an RT/real-time PCR with a light Cycler System using DNA binding dye SYBR Green I, and immunoblotting with AR polyclonal antibody (Santa Cruz Biotechnology, Inc, Santa Cruz, CA, USA), as reported previously [10,12].

GeneChip microarray assay

The VSMCs above were cultured until a sub-confluent state was achieved. The medium was then replaced with fetal bovine serum (FBS)-free and phenol red-free medium to arrest cell proliferation. After 24 h, the medium was replaced again with phenol red-free and FBS-free medium in the presence of testosterone (10 nM) or vehicle (0.1% ethanol). After incubation for 2 h, the cells were subsequently subjected to total RNA extraction for microarray analysis. Isolated total RNA was labelled as described in the Affymetrix (Santa Clara, CA, USA) GeneChip Expression Analysis Technical Manual (revision 3), as previously described [10]. The ratios represent the values up- or down-regulated by 10 nM testosterone treatment compared with control. We independently repeated the same experiment twice. Genes for which the average ratios increased more than 1.5-fold in both experiments using 10 nM testosterone treatment were considered up-regulated via AR when compared with control values [13]. When studying the potential functions of these genes, we used the homepage of the HUGO Gene Nomenclature Committee (http://www.gene.ucl.ac.uk/nomenclature, accessed 28 March 2006) for further examination of whether any had been previously reported to be involved in cell proliferation and to be associated with androgen effects. In this study, among the genes that were found to be significantly induced by testosterone treatment by microarray analysis, we regarded a gene that was up-regulated, and was known to be associated with both cell proliferation and androgenic effects, as a target gene.

Quantitative real-time PCR

After achieving sub-confluence and following growth arrest states of the VSMCs as described above, the medium was replaced again with phenol red-free and FBS-free F12-K medium with testosterone (10 nM), testosterone (10 nM) with flutamide, an AR-blocker (100 nM), or vehicle. After incubation for 2 h, the cells were subsequently subjected to total RNA extraction for RT/real-time PCR analysis, described previously [10]. mRNA levels for the target gene *PTOV1* were determined in each VSMC as a ratio relative to glyceraldehyde-3-phosphate dehydrogenase (*GAPDH*), and evaluated as a ratio (%) compared with that of each control cDNA. The analyses with real-time PCR were repeated three times. Table 1 summarizes the primers used [14].

siRNA preparation, transfection, and cell count assay

Small interfering RNAs (siRNAs) corresponding to *PTOV1* (Table 2) were synthesized based on results of a previous report, and were transfected into the VSMCs [15]. These VSMCs were seeded in a 24-well plate at an initial concentration of 50 000 cells/well with F-12K medium containing 2% FBS and were cultured until a sub-confluent status was achieved. The medium was then replaced with phenol red-free and FBS-free medium to arrest cell proliferation. After 24 h, transfection experiments of siRNA for endogenous gene targeting (10 nM or 100 nM) were carried out using RNAiFect™ transfection reagent (Qiagen, Valencia, CA, USA). After transfection, the cells were incubated in phenol red-free medium containing 2% dextran-coated, charcoal-stripped FBS with testosterone (10 nM) or vehicle (0.1% ethanol) for 24 h. We measured the number of cells in each sample as described above with Cell Counting Kit-8 system (Wako, Tokyo, Japan) after incubation for 48 h. We also examined the number of cells treated with

Table 1. Primer sequences used in RT-PCR analysis

cDNA	Sequence	Size (bp)
AR	Forward 5′-CTCACCAAGCTCCTGGACTC-3′ Reverse 5′-CAGGCAGAAGACATCTGAAG-3′	246
GAPDH	Forward 5′-TGAACGGGAAGCTCACTGG-3′ Reverse 5′-TCCACCACCCTGTTGCTGTA-3′	307
PTOV1	Forward 5′-CACCATCCCTCCATGTTGCTG-3′ Reverse 5′-TCTTCATTGGCCTCATCCCC-3′	250

Table 2. Sequences used in siRNA transfection analysis

cDNA	Sequence
PTOV1	Sense r(CAACAAGUUUCUGGCAUGG)dTdT Antisense r(CCAUGCCAGAAACUUGUUG)dTdT
Negative control	Sense r(UUCUCCGAACGUGUCACGU)dTdT Antisense r(ACGUGACACGUUCGGAGAA)dTdT

The target gene in this study (*PTOV1*) was determined by microarray analysis. The sequences of *PTOV1* siRNAs are based on a previous report [15].

transfection of negative control siRNA with scrambled sequences (Table 2), and treated with testosterone (10 nM) or vehicle. In order to evaluate transfection efficiency, we examined relative *PTOV1* mRNAs levels in these cells at 24 h after transfection of the specific siRNAs. The mRNA levels in each VSMC were calculated as a ratio relative to *GAPDH*, and were normalized to the ratio after transfection of negative control siRNA (10 nM).

Quantitative RT-PCR analysis of *PTOV1* mRNA expression in human aorta

Samples of human abdominal aorta were collected at autopsy from patients without a history of hormone replacement therapy. Autopsies were performed on 32 subjects (16 male, 16 female; mean 60.7 ± 3.3 years) in Tohoku University Hospital (Sendai, Japan) within 2 h post mortem. The Ethics Committee at Tohoku University School of Medicine approved the research protocol for this study. Aortic specimens were tentatively classified into the following four groups according to the sex of the deceased patient and degree of atherosclerosis, as previously described: group A = male, mild atherosclerosis, corresponding to groups I–III in the American Heart Association (AHA) classification; group B = male, advanced atherosclerosis, corresponding to groups IV–VI in the AHA classification; group C = female, mild atherosclerosis; and group D = female, advanced atherosclerosis) [10,11]. The distribution of the cases among these groups was as follows: A, 8 cases (mean 44.3 ± 10.6 years); B, 8 cases (mean 71.3 ± 3.7 years); C, 8 cases (mean 52.0 ± 3.9 years); and D, 8 cases (mean 75.0 ± 2.1 years), respectively. For RT/real-time PCR analysis, these specimens were treated according to our previous report [10]. The mRNA levels for *PTOV1* and *AR* in each sample are given as a ratio relative to *GAPDH*, and evaluated as a ratio (%) compared with that of each control cDNA.

Immunohistochemical analysis for PTOV1 protein expression in human aorta

Details of immunohistochemical procedures have been previously described [10,11]. We used immunostaining with diaminobenzidine (DAB) for immunohistochemical analysis of PTOV1 protein (using a monoclonal anti-human PTOV1 antibody; Novocastra Laboratories, Newcastle, UK) and AR (using a monoclonal antibody for human AR; Dako Corporation, Carpinteria, CA, USA). We also used double immunostaining with DAB and Vector Blue as colorimetric reagents, with a combination of monoclonal antibodies for α-smooth muscle actin (α-SMA; Dako Corporation), for macrophages (PG-M1, Dako Corporation), and for leukocytes (human leukocyte common antigen antibody (LCA; Dako Corporation) in adjacent tissue sections. After determining the areas for evaluation by simultaneous observation using a multi-headed light microscope, three authors (YN, TS, and HS) independently evaluated immunoreactivity. Scoring of immunoreactivity was performed based on our previous reports with some modifications [10,16]. When PTOV1 protein was immunolocalized to the cytoplasm, the relative immunoreactivity in each specimen was classified into the following three groups: 2 = more than 50% positive cells; 1 = more than 10% and less than 50% positive cells; and 0 = negative or less than 10% positive cells, respectively [16]. When PTOV1 protein immunoreactivity was detected in the nuclei, the relative immunoreactivity in each specimen was evaluated by the percentage of immunoreactivity, ie the labelling index (LI) [10]. When inter-observer differences were >5%, the three aforementioned authors re-evaluated these discrepant immunostained slides simultaneously using a multi-headed light microscope, and the mean value was obtained.

Statistical analysis

Values for all results were given as the mean ± standard error of the mean (SEM). Results of quantitative RT-PCR, cell count assay, and the relative immunoreactivity for protein in the nuclei were analysed using one-way analysis of variance followed by unpaired *t*-test for comparisons between two groups. Results of immunohistochemistry of cytoplasmic protein were analysed using the χ^2-test. Statistical differences between immunoreactivity for PTOV1 protein and AR were evaluated using Spearman's rank correlation. A p value <0.05 was considered significant in this study.

Results

Characterization of two VSMC cell lines

By RT-PCR analysis, both HUVS-112D cells and T/G HA-VSMC cells expressed *AR* mRNA (Figure 1A). In addition, AR protein was demonstrated in both of these cell lines by immunoblotting analysis (110 kD) (Figure 1B). Relative levels of AR mRNA and protein expression in these cells were approximately 5–10% of those in LNCaP cells that were examined in parallel (data not shown).

Gene chip microarray assay

Table 3 summarizes 11 genes that were up-regulated by testosterone treatment in both types of VSMC in duplicated microarray analysis. Among these genes, human prostate tumour overexpressed protein 1, ie *PTOV1* was detected in both of these VSMCs. Recently, *PTOV1* has been reported to be induced by androgen and to be involved in cell cycle regulation [14,15,17]. *AGTR2* was also reported to be associated with androgenic effects, but it is unknown whether *AGTR2* is involved in cell growth [18]. Therefore we focused our subsequent studies on *PTOV1* as

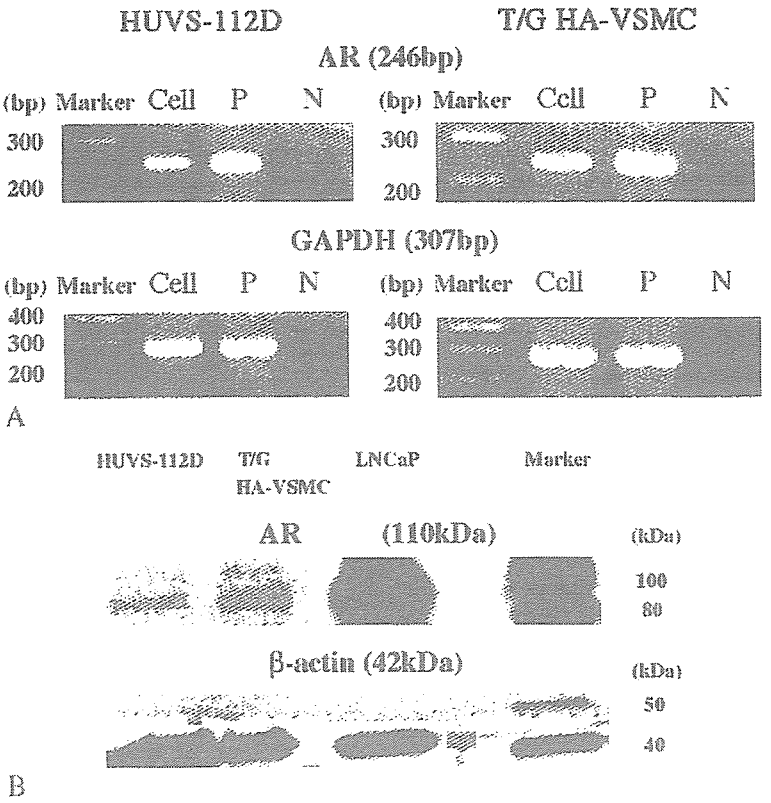

Figure 1. (A) Results of RT/real-time PCR analysis for *AR* and *GAPDH* in two cultured human VSMCs (HUVS-112D, and T/G HA-VSMC), positive controls, and negative controls. Cell = each type of cultured vascular smooth muscle cell; P = positive control (LNCaP prostate cancer cell line); N = negative control (no cDNA), respectively). (B) Immunoblotting analysis of AR and β-actin in HUVS-112D, T/G HA-VSMC, and LNCaP cells. Total protein was extracted, and 60 μg protein from each cell was loaded. Immunoblotting analysis demonstrated both AR (110 kD) and β-actin protein (42 kD) in all cells

Table 3. Ratios of gene expression determined by GeneChip microarray analysis after testosterone treatment of cultured VSMCs for 2 h

Gene symbol	HUVS-112D	T/G HA-VSMC	Function	Association with androgen (reference)
PAK7	3.9	3.6	Neurite development	Unknown
PIK3R4	1.7	3.3	Cell signalling	Unknown
CELSR1	1.9	3.1	Cell adhesion	Unknown
CACNA1G	2.5	2.9	Calcium channel	Unknown
AGTR2	2.2	2.5	Regulator of aldosterone secretion	Koike *et al* [18]
INVS	2.7	3.6	Renal tubular development	Unknown
GPR77	3.5	2.6	Cell signalling	Unknown
CASP10	3.3	2.8	Apoptosis	Unknown
APMS1	2.1	2.5	Formation of cell structure	Unknown
TIA-2	1.7	2.7	Membrane glycoprotein	Unknown
PTOV1	1.8	2.0	Cell growth/mitogenesis	Benedit *et al* [14]

'Ratios' represent the mean ratios of expression levels of each gene mRNA in duplicate experiments compared with control.

an androgen-responsive gene possibly involved in the proliferation of human VSMCs.

PTOV1 mRNA expression in VSMCs after androgen treatment

Testosterone significantly increased *PTOV1* mRNA levels in AR-positive VSMCs compared with controls in both of these cell lines ($p < 0.05$) (Figure 2). However, testosterone with flutamide, an AR-blocker (100 nM), did not increase its mRNA expression in either of these cells ($p < 0.05$) (Figure 2).

PTOV1 siRNA transfection and cell proliferation assay

Quantitative RT-PCR analysis demonstrated that *PTOV1* mRNA levels were decreased in a dose-dependent manner in the cells transfected with *PTOV1* siRNAs (Figure 3A). After transfection of negative

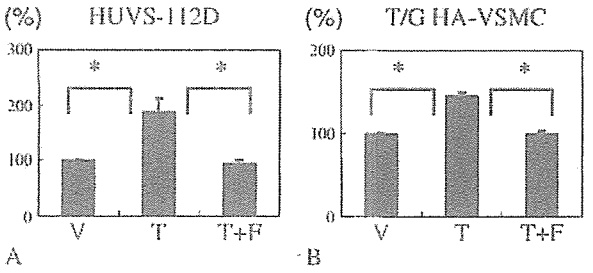

Figure 2. Results of RT/real-time PCR analysis for *PTOV1* in HUVS-112D (A) and T/G HA-VSMC cells (B) among cells treated with vehicle (V) (control), testosterone (T) alone (10 nM), and T (10 nM) with flutamide (F), an AR-blocker (100 nM), respectively after 2 h (*$p < 0.05$)

control siRNA (10 nM), testosterone promoted cell proliferation significantly in both of these cell lines ($p < 0.05$) (Figure 3B). However, testosterone with transfection of *PTOV1* siRNA (10 nM and 100 nM) did not increase cell proliferation in these two cell lines (Figure 3B).

PTOV1 mRNA expression in human aorta

The results of RT/real-time PCR analysis demonstrated the presence of specific single bands for *AR* and *PTOV1* in human aorta (Figure 4A). The relative abundance of *PTOV1* mRNA was significantly greater in male aorta with a mild degree of atherosclerotic changes (group A) than in those of other groups (groups B, C, and D)($p < 0.05$) (Figure 4B). The relative abundance of *AR* mRNA was also significantly greater in male aorta with a mild degree of atherosclerotic change (group A) than in male aorta with a severe

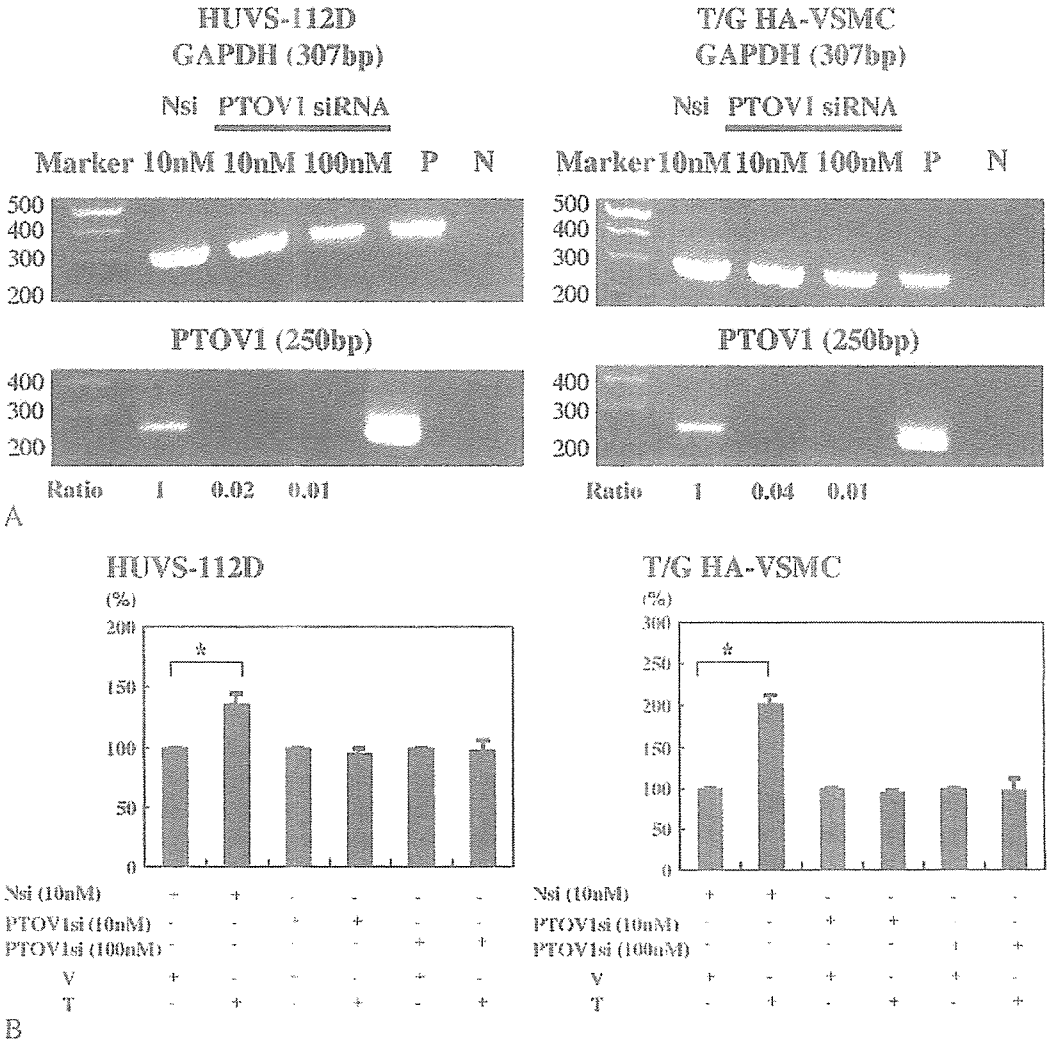

Figure 3. (A) Expression of *PTOV1* and *GAPDH* mRNAs at 24 h after transfection of *PTOV1* siRNA (10 nM or 100 nM) or negative control siRNA (Nsi) (10 nM) in HUVS-112D and T/G HA-VSMC cells detected by real-time PCR, respectively. *GAPDH* mRNA expression was monitored as an internal control. The ratio of *PTOV1/GAPDH* was calculated and values were normalized to the ratio obtained from the negative control transfection of Nsi (10 nM). P = positive controls (LNCaP prostate cancer cell lines); N = negative controls (no cDNAs), respectively. (B) The relative levels of cell numbers in HUVS-112D and T/G HA-VSMC cells among cells treated with vehicle (V) (0.1% ethanol) and testosterone (T) alone (10 nM) after transfection of *PTOV1* siRNA (PTOV1si) (10 nM or 100 nM) or negative control siRNA (Nsi) (10 nM) (*$p < 0.05$)